B3

Chevrel Phases

Damian P Hampshire

B3.1 Introduction

Chevrel phase superconductors are a class of materials that have generated enormous interest in the superconductivity community. There are more than 100 different Chevrel phase compounds that exhibit a wide range of properties of both fundamental and technological interest. They have the chemical formula $M_xMo_6X_8$, where M can be one of more than 25 different elements that are mono-, di- or trivalent, x can range from 1 to 4, and X is usually one of the chalcogenides (S, Se or Te). The structure can incorporate elements of different size, concentration and oxidation state. Some of the most intensively studied Chevrel phase materials with superconducting critical temperatures above 2 K are listed in Table B3.1 (Fischer et al., 1975b; Shelton et al., 1976; Chevrel and Sergent, 1982; Fischer and Maple, 1982a, b). Figure B3.1 shows the critical temperature, magnetic ordering temperature and some structural properties of Chevrel phase materials with rare-earth ions (Ishikawa et al., 1982; Peña and Sergent, 1989; Pena et al., 1999; Perrin and Perrin, 2012; Pena, 2015).

The Chevrel phase compounds were discovered in 1971 (Chevrel et al., 1971). Interest has focused on the $PbMo_6S_8$ and $SnMo_6S_8$ materials with high upper critical fields (B_{C2} ~ 40 – 60 T) and T_C values of ~ 12–15 K. The B_{C2} values of these Chevrel phase compounds lie between those of the high-temperature copper oxide superconductors (e.g. $Bi_2Sr_2Ca_2Cu_3O_x$) and the intermetallic low-temperature superconductors (e.g. Nb_3Sn), which means the superconducting coherence length is sufficiently long to reduce the effects of granularity found in high-temperature superconductors but sufficiently short for very high-field applications. Powder-in-tube wires have been fabricated (Cheggour et al., 1997; Cheggour et al., 1998; Eastell, 1998) with a reasonably high critical current density (J_C) in high magnetic fields (Yamasaki et al., 1992; Seeber et al., 1995; Cheggour et al., 1997) in single lengths up to 1 km long (c.f. Chapter B3.3.5). This has opened the possibility that these materials could be used in high-field applications operating at magnetic fields significantly above 25 T (Cheggour et al., 1998). Nevertheless, a further increase in J_C is probably required for these materials to compete with Nb_3Sn, which is already well-established, or for them to attract industrial R&D interest away from developing the HTS materials, although as discussed below, there are magnet design and stability issues (i.e. rapid quench detection) that may eventually favour use of Chevrel phase materials.

The fundamental interest in these materials has long included studies of the many Chevrel phase compounds that include rare-earth elements that are found to exhibit the coexistence of superconductivity and long-range magnetic order (Matthias et al., 1972; Foner et al., 1974; Fischer, 1978; Niu et al., 2001). Also their presence on the Uemura plot (Uemura et al., 1991) has opened the question of whether Chevrel phase compounds are really Bardeen–Cooper–Schrieffer (BCS) superconductors or are better considered as belonging to the class of [non-BCS (Bardeen et al., 1957; Abrikosov, 2000)] superconductors that includes the cuprates and is characterised by relatively high critical temperature for such small n_s/m^* (carrier density/effective mass) (Uemura et al., 1991).

We note that there is a huge family of $M_6X_{8-x}X'_x$ cluster compounds (Gougeon et al., 1984; Perrin and Perrin, 2012; Pena, 2015) that includes Chevrel phase materials with the general formula $M_{2n-2}M'_{6n}X_{6n-x+2}X'_x$, where the $M'_6X_{8-x}X'_x$ clusters are the basic structural building block. One can consider Chevrel phase materials as $Mo_{6n}X_{6n-x+2}X'_x$ cluster compounds connected in a three-dimensional framework and the other family compounds as connected in 2-, 1- and 0-dimensional frameworks. Some of these compounds include some relatively high-temperature superconductors such as $Mo_6S_6I_2$ (T_C = 14 K) (Perrin and Perrin, 2012; Pena, 2015) although the in-field properties are not well studied. Many of these materials have also been intensively investigated at room temperature, because of their potential to be electrode materials in catalysts (Benson et al., 1995; Kamiguchi et al., 2013; Kamiguchi et al., 2015), thermoelectric devices (Caillat et al., 1999; Nunes et al., 1999;

TABLE B3.1 The Critical Temperature of Chevrel Phase Materials and Related Compounds: the Critical Temperature (T_C) (Fischer et al., 1975a; Shelton et al., 1976); the Rhombohedral Angle and the Rhombohedral Lattice Parameter (Fischer and Maple, 1982a) (Chevrel and Sergent, 1982) (Perrin et al., 1979).

Compound	*Tc*	Rhombohedral lattice parameter (Å)	Rhombohedral angle
		Sulphides	
$PbMo_6S_8$	15	6.55	89.4
$SnMo_6S_8$	13	6.52	89.7
$AgMo_6S_8$	9	6.48	92.0
$ScMo_6S_8$	3.6	-	-
YMo_6S_8	3.0	6.45	89.5
VMo_6S_8	8.2	-	-
$NbMo_6S_8$	3.5	-	-
$LaMo_6S_8$	7.1	6.51	88.9
Mo_6S_8	1.6	6.43	91.6
$Cu_{1.8}Mo_6S_8$	11	6.48	94.9
$C_{3.2}Mo_6S_8$	6.4	-	-
$Cu_4Mo_6S_8$	< 1	6.59	95.6
$Cd_{1.1}Mo_6S_8$	3.5	6.52	92.8
$Li_4Mo_6S_8$	4.4	6.62	94.5
$Mg_{1.14}Mo_6S_8$	3.5	6.51	93.6
$Cu_{1.2}Mo_6S_8$	5.6	-	-
$Zn_{1.1}Mo_6S_8$	3.6	6.49	94.7
$Cu_2Mo_6S_6O_2$	9	6.54	95.51
$PbMo_6S_8O_2$	11.7	6.52	88.98
		Selenides	
$PbMo_6Se_8$	6.7	6.81	89.23
$SnMo_6Se_8$	6.8	6.78	89.6
$AgMo_6Se_8$	6	6.73	91.4
$Cu_{2.8}Mo_6Se$	6	6.79	94.9
		Binaries and doped binaries	
Mo_6Se_8	6.4	6.66	91.58
$Mo_6Se_{4.8}Te_{3.2}$	2.7	-	-
Mo_6Se_7Br	7.1	-	-
Mo_6Se_7Cl	7.0	-	-
$Mo_6S_6Br_2$	13.8	6.50	94.43
$Mo_6S_6I_2$	14.0	-	-
Mo_6Se_7I	7.6	-	-
$Mo_6Te_6I_2$	2.6	-	-
$Mo_4Re_2Te_8$	3.5	-	-
$Mo_6S_{4.8}Te_{3.2}$	2.7	-	-

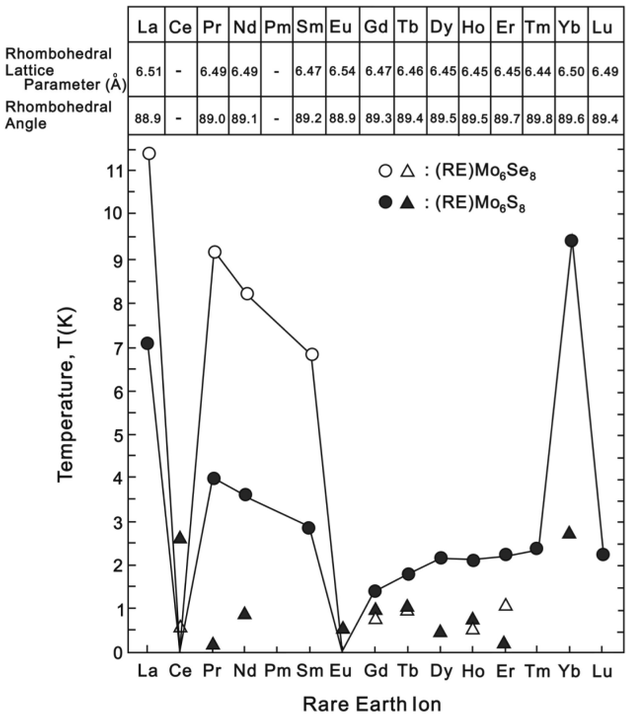

FIGURE B3.1 The rare-earth Chevrel phase superconductors: the critical temperature (T_C: o, •), the magnetic ordering temperatures (Δ, ▲) (Fischer et al., 1975a; Shelton et al., 1976; Ishikawa et al., 1982; Peña and Sergent, 1989); the rhombohedral angle and the rhombohedral lattice parameter (Chevrel and Sergent, 1982) (Pena, 2015). No large high-quality single crystals of heavy rare-earth selenides (i.e. Gd–Yb) have yet been obtained (Pena et al., 1999); two phase samples with Mo_6Se_8 (T_C ~ 6.4 K) are produced.

Fleurial et al., 2002; Ohta et al., 2009b; Ohta et al., 2009a; Goncalves and Godart, 2014) and batteries (Aruchamy et al., 1994; Mitelman et al., 2007; Levi et al., 2010; Kumta et al., 2015; Cheng et al., 2016), most obviously using magnesium in batteries (Aurbach et al., 2000) but also using calcium (Smeu et al., 2016) and aluminium (Geng et al., 2015). In this article, although we point to developments made during that research, it remains broadly focussed on superconducting Chevrel phase materials that may be of use in potential high-field superconducting applications.

B3.2 Structural Properties

The majority of superconducting Chevrel phase superconductors are trigonal with space group $R\bar{3}$ and can be described using either the hexagonal or rhombohedral structure (Nespolo et al., 2018). Figure B3.2 provides a schematic of the structure for $M_xMo_6X_8$, where M is Pb and X is S. The Pb occupies the origin of the unit cell and the tightly bound Mo_6S_8 cluster lies at the centre of the rhombohedron. The clusters are rotated through ~ 25° about the [111] and thus form the channels in which the M atoms are located. The Mo forms an octahedron such that each Mo atom is slightly outside the middle of the faces of the S-cube. The Mo_6S_8 is bound together as a cluster with weak intercluster Mo–Mo bonds. The 4d orbitals of the Mo ions are well extended so they favour the metallic bond. The edges of the sides of the rhombohedron are equal and inclined at the same angle (~90°) which means the structure can also be considered as a slightly distorted pseudo-cubic structure as shown in the bottom of Figure B3.2 (Uchida and Wakihara, 1991). In this cubic description, the Pb

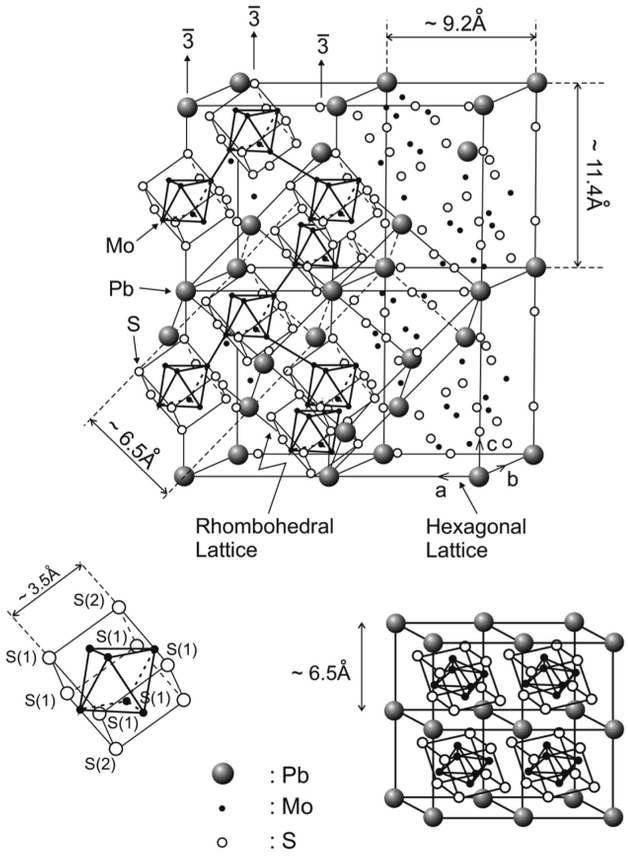

FIGURE B3.2 A schematic of the rhombohedral and pseudo-cubic structure of $PbMo_6S_8$ (Uchida and Wakihara, 1991).

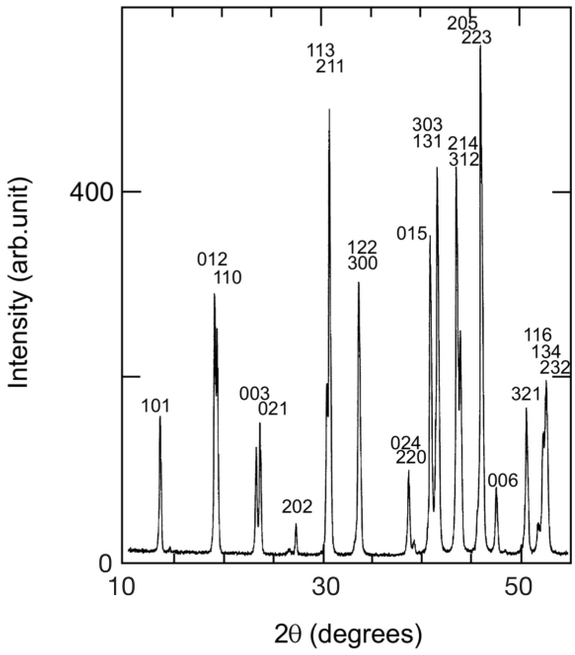

FIGURE B3.3 CuKα powder x-ray diffraction powder pattern for a typical single phase $PbMo_6S_8$ sample (Niu et al., 2002).

is almost at the centre of the central cube. At the corners of the central cube are the tightly bonded Mo_6S_8 clusters. The sides of the unit cell are about 6.5 Å and those of the Mo_6S_8 cluster about 3.5 Å. The bond lengths of the Mo_6X_8 cluster in ternary Chevrel phase materials are generally similar to those of the binary parent compounds. All the compounds have metal–metal bonds within the cluster. Important structural features that affect superconducting properties are the Mo–Mo intracluster distance, which can vary from 2.7 Å to 2.9 Å and is correlated with the number of valence electrons on the Mo_6S_8 cluster (Yvon and Paoli, 1977), and the intercluster distance, which can vary from 3.1 Å to 3.6 Å. The iono-covalent intercluster bond can be doped from an insulating state to produce a metallic bond that is superconducting.

Chevrel phase compounds can be divided into two types: stoichiometric and non-stoichiometric:

i. Stoichiometric compounds of $M_xMo_6X_8$ contain large cations such as Pb, Sn, Ag and the rare-earth elements. The structure basically accommodates 1 M ion in one of six positions which are sufficiently close together to appear as a single site. There is a narrow range of M solubility. All stoichiometric compounds crystallise in the trigonal structure at high temperatures with the rhombohedral angle between 88° and 90°. A typical x-ray diffraction pattern for $PbMo_6S_8$ is shown in Figure B3.3 (Niu et al., 2002). The positions of the main diffraction lines and h, k, l indices for the Chevrel phase compound $PbMo_6X_8$ and the most important second phases are given in Table B3.2.
ii. Non-stoichiometric compounds occur with small ions such as Li, Cu and Zn. The rhombohedral angle is between 92° and 95°. The structure can accommodate more than one ion. Figure B3.4 shows the possible sites for Cu in the inner cube of the Chevrel phase structure (Chevrel and Sergent, 1982). There are six inner sites and six outer sites. The sites for the small cations depend on the particular cation (Mancour-Billah and Chevrel, 2003) (Pena et al., 2009). With In for example, only the six inner sites are available. At sufficiently low temperatures, the M ion will freeze in one position which breaks the trigonal symmetry and can favour a phase transition to a triclinic structure.

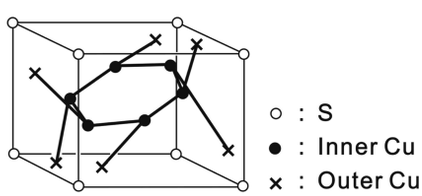

FIGURE B3.4 The possible sites for Cu in the inner cube of $Cu_XMo_6S_8$ [adapted from (Chevrel and Sergent, 1982)].

TABLE B3.2 The x-Ray Diffraction Peaks for $PbMo_6S_8$ and the Strong Intensity Lines (> 10%) for the Important Impurity Phases (Mo, MoS_2, Mo_2S_3, Pb, PbS and S). Radiation: CuKα1, λ = 1.54056 Å

2-theta	Int.	h k l	2-theta	Int.	h k l	2-theta	Int.	h k l
	$PbMo_6S_8$			MoS_2			Pb	
13.612	50	1 0 1	14.38	100	0 0 2	29.55	100	1 0 0
19.153	100	0 1 2	32.67	22	1 0 0	33.66	80	1 0 1
19.364	80	1 1 0	33.51	12	1 0 1	42.82	75	-
23.303	50	0 0 3	35.87	10	1 0 2	52.23	75	1 1 0
23.700	40	0 2 1	39.53	58	1 0 3	57.95	75	1 0 3
-	-	2 0 2	44.15	11	0 0 6		PbS	
-	-	1 1 3	49.78	29	1 0 5	25.96	84	1 1 1
30.753	100	2 1 1		Mo_2S_3		30.07	100	2 0 0
-	-	1 2 2	10.48	10	0 0 1	43.06	57	2 2 0
33.666	80	3 0 0	16.28	95	1 0 1	50.97	35	3 1 1
38.730	20	0 2 4	21.06	36	0 0 2	53.41	16	2 2 2
-	-	2 2 0	29.61	35	$\bar{2}$ 0 1		S	
40.971	40	0 1 5	29.73	26	0 1 1	16.59	10	1 2 1
-	-	3 0 3	31.66	46	1 1 0	19.62	17	2 1 2
-	-	1 3 1	31.66	46	0 0 3	22.08	17	2 2 0
-	-	2 1 4	32.33	16	$\bar{1}$ 1 1	23.28	100	2 2 2
43.938	40	3 1 2	32.89	12	$\bar{2}$ 0 2	23.58	23	1 3 2
-	-	2 0 5	34.46	19	1 1 1	24.30	25	1 2 5
-	-	2 2 3	35.09	37	0 1 2	25.37	23	1 3 3
-	-	0 0 6	36.39	11	$\bar{1}$ 1 2	26.05	49	0 2 6
-	-	3 2 1	39.04	28	$\bar{2}$ 0 3	26.84	34	3 1 1
-	-	1 1 6	40.16	58	1 1 2	27.87	36	2 0 6
-	-	1 3 4	40.72	39	2 0 2	28.86	36	1 3 5
-	-	2 3 2	41.03	24	$\bar{2}$ 1 1	31.60	24	0 4 4
	Mo		42.27	21	$\bar{1}$ 0 4	34.27	13	4 0 0
40.51	100	1 1 0	42.93	100	0 1 3	34.37	13	1 3 7
58.60	16	2 0 0	42.93	100	0 0 4	35.06	11	3 3 3
			43.58	51	$\bar{2}$ 1 2	37.17	11	4 0 4
			46.18	23	$\bar{3}$ 0 2	42.84	12	3 1 9

Source: [taken from the International centre for Diffraction data (Fischer and Maple, 1982a).]

The structural transformation from high-temperature rhombohedral to triclinic ($P\bar{1}$) between 100 K and 140 K (Jorgensen et al., 1987) has been observed in $PbMo_6S_8$ (Jorgensen and Hinks, 1985) using neutron scattering. Synchrotron data show a much smaller triclinic distortion, which suggests that sample preparation [possibly oxygen contamination (Wolf et al., 1996)] affects the low-temperature transformation (François et al., 1994). The triclinic phase is the stable low-temperature phase for the non-superconducting divalent (Eu^{2+}, Ba^{2+}, Sr^{2+} and Ca^{2+}) molybdenum sulphide Chevrel phases (Jorgensen and Hinks, 1986). Steric and electronic effects (principally charge transfer to the Mo_6S_8 cluster) are important in determining the equilibrium structure (Pena et al., 1999). Materials with the highest T_C are those metallic compounds adjacent to a structural instability. They may be in a mixed-phase region consisting of both a superconducting rhombohedral phase and an insulating triclinic phase (Jorgensen and Hinks, 1986). The structural instability can result either from changing the cation (chemical pressure) or applying pressure directly (Jorgensen et al., 1987). As discussed below in the context of the Uemura plot (Uemura et al., 1991), a similar structural instability is found in some of the A15 superconductors which undergo a shear martensitic transformation at some temperature above T_C (Batterman and Barrett, 1964).

The structure of $Cu_xMo_6S_{8-y}$ has been studied in detail below 300 K. Four different low-temperature modifications of the rhombohedral phase have been observed (Flükiger and Baillif, 1982). For $x = 1.2$, $T_C = 5.6$ K; for $x = 1.8$, $T_C = 11$ K; for $x = 3.2$, $T_C = 6.4$ K and for $x = 4$, the material is not superconducting (Niu et al., 2001). Less detailed studies have also been completed on Ni molybdenum sulphides and selenides.

Solid solutions of Chevrel phase materials can generally be fabricated if the end compounds exist. The solution can either occur with the chalcogenides (e.g. $M_xMo_6Se_{8-x}S_x$) or with the M-elements (Fischer, 1978). Neutron measurements show that in the ternary Pb- and Sn Chevrel phase sulphides, oxygen can substitute for sulphur which strongly affects the superconducting properties (Hinks et al., 1983). Of note is the $EuMo_6Se_8$ compound in which either a vacancy or oxygen substitution for Se causes the Eu to move 0.9 away from the usual central site (Le Berre et al., 1998a). Low-level doping of 1–1.5 at% Pb or rare-earth ions into the Chevrel phase binary compound Mo_6Se_8 has also been reported (Le Berre et al., 1997; Corrignan et al., 1999).

There is some limited work on structures that occur at very high pressures and temperatures (30–80 kbar and 1200°C). Preliminary work suggests that a metastable structure can be formed in the $PbMo_6S_8$ system (Khlybov et al., 1986) at high pressure which has a T_C enhanced by about 1 K but a severely reduced upper critical field (~7 T).

B3.3 Phase Diagrams and Fabrication

The high vapour pressure of the Pb and S makes accurate phase studies difficult. Very careful exclusion of oxygen and water during material fabrication is required to avoid oxygen substituting for the sulphur in the Mo_6S_8 cluster (Hinks et al., 1984) and is necessary for reliable comparisons between structure/composition and superconducting properties. Argon should be used rather than argon–nitrogen since trapped nitrogen can form MoN. Chevrel phase materials start decomposing under vacuum or low helium pressure above 650°C (Miraglia et al., 1987). Most of the important compounds melt in the temperature range from 1500°C to 2000°C, and the vapour pressure of the S or Se (Pb, Sn) is high (Peña and Sergent, 1989; Horyn et al., 1994). The Pb, Sn, Ag and rare-earth sulphide and selenide Chevrel phase materials melt peritectically (Fischer and Maple, 1982a). To make single crystals of the metallic superconductors, a typical off-stoichiometric composition of $Pb_{1.2}Mo_7S_8$ (Flükiger and Baillif, 1982) or for rare-earth

sulphides compounds, $RE_{11}Mo_{38}S_{51}$, is used (Holtzberg et al., 1984; Horyn et al., 1989; Peña and Sergent, 1989). These compositions are chosen to produce an excess of the binary chalcogenide which minimises formation of the Mo_2S_3 phase that competes with the Chevrel phase. Figure B3.5 (upper) shows a schematic of the phase diagram for $PbMo_6S_8$ found at ~ 1000°C (Krabbes and Oppermann, 1981; Yamamoto et al., 1985). The Mo_2S_3 phase does not form at lower temperatures (Yamasaki and Kimura, 1986). The high-temperature phase diagram characteristic of the rare-earth compounds is shown in Figure B3.5 (lower) (Peña and Sergent, 1989). Material can be simply cooled from above its melting point to produce single crystals. The final product is generally single crystals in a binary chalcogenide crust which can be separated using HCl diluted with ethyl alcohol (≈ 20 vol.% HCl). The natural cleavage planes are the (100) and (110) crystallographic planes (Holmgren et al., 1987). The Cu and Ni sulphide Chevrel phase materials form congruently so that relatively large single crystals can be formed from a stoichiometric melt. In selenium-based materials, only single crystals of the light rare earths have been produced (Horyn et al., 1994; Horyn et al., 1996; Pena et al., 1999; Le Berre et al., 2000). In heavy rare-earth selenides, RE deficiency produces a two-phase sandwich structure of doped binary Mo_6Se_8 and $REMo_6Se_8$ (Le Berre et al., 1995; Horyn et al., 1996; Le Berre et al., 1996; Pena et al., 1999; Hamard et al., 2002).

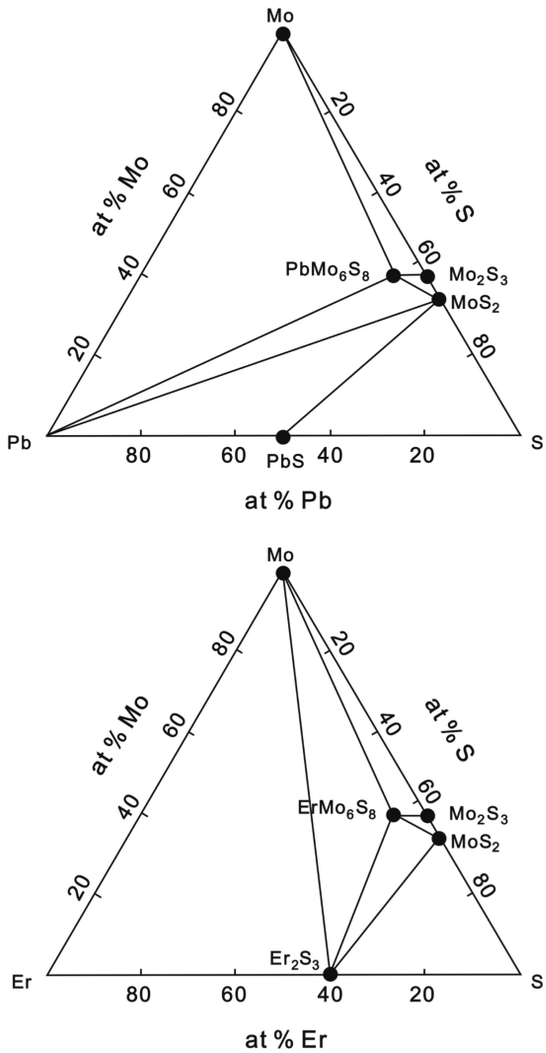

FIGURE B3.5 A schematic of the phase diagram for $PbMo_6S_8$ (upper) (Krabbes and Oppermann, 1981; Yamamoto et al., 1985) and $ErMo_6S_8$ (lower) at temperatures above 1000°C (Peña and Sergent, 1989).

A number of authors have studied the phase diagrams of the $Pb_xMo_6S_{8-y}$ at 900°C (Yamasaki and Kimura, 1986) and ~ 1000°C (Krabbes and Oppermann, 1981; Yamamoto et al., 1985). There is no general agreement about the composition of the Chevrel phase material in the single-phase region although many studies show the presence of a small amount of sulphur defects, consistent with high-resolution electron microscopy (HREM) studies (Kang et al., 1994). Although as long as there is no oxygen contamination, the onset of T_C is in the range of 14–15 K, the sulphur stoichiometry is very close to 8, and Pb deficiency is present (Decroux et al., 1993). Chevrel phase materials have been fabricated at high pressure (typically up to 2000 atmospheres) to increase density and connectivity. It has been suggested that this enhances the effect of oxygen contamination since the material is pushed into a two-phase Chevrel phase + MoS_2 region (Ingle et al., 1998). Limited work has been completed on decomposition. Since $PbMo_6S_8$ can be formed between 450°C and 1650°C, it is reasonable to assume that the structure is very stable. Electron beam–induced decomposition has been observed in $Ni_2Mo_6S_8$ first showing increased disorder and then, after time, reduction of the Mo_6S_8 clusters giving regions of Mo, Mo–Ni alloy and sulphides (Kang et al., 1994). A detailed investigation of the phase diagram at 1200°C in La–Mo–Se has also been completed and the correlation between structural and superconducting properties investigated (Horyn et al., 1996; Le Berre et al., 1998b; Peña et al., 1998).

Amongst the family of cluster compounds related to Chevrel phase materials (Perrin and Perrin, 2012; Pena, 2015), substitutions of Br, I and O for the X-element and mixed sulphur–selenium compounds have been fabricated. The Br, I and O substitutions can increase T_C. Replacing S by Se or vice versa immediately reduces T_C producing a minimum when there are equal quantities of each element (e.g. $PbMo_6Se_4S_4$). Most materials in which the Mo-element has been substituted (e.g. Nb, Ta, Re, Ru and Rh) are not superconducting (Chevrel and Sergent, 1982).

Fine grain, well-connected bulk samples are required for high J_C applications. Soft chemistry methods have been used to produce ultrafine and amorphous precursors (PbS, MoS_2 and Mo) (Chevrel et al., 1974; Even-Boudjada et al., 1998b, a). Alternatively very fine grains of the binary compound Mo_6S_8, which are almost oxygen free, can be formed by leaching the Ni or Li ions out of the parent Chevrel phase compound using HCl (Selvam et al., 1992; Even-Boudjada et al., 1999), where the Ni or Li ions can migrate over distances of ~100 μm. The fine

Mo_6S_8 grains can then be used in powder route fabrication of fine grain bulk Chevrel phase materials by reacting with PbS or SnS (Cheggour et al., 1993; Selvam et al., 1993). Fast cheap microwave synthesis can also be effective (Murgia et al., 2016).

Thin films have been fabricated using a range of different deposition techniques including sputtering (Koo et al., 1995) and laser ablation (Decroux et al., 1999) as well as spin coating (Boursicot et al., 2012). Multifilamentary wires have also been produced (Sergent et al., 1984; Willis et al., 1995; Flükiger, 2010), as have monocore wires with Ag (Luhman and Dew-Hughes, 1978), Ta (Goldacker et al., 1989a) and Mo sheathing (Yamasaki et al., 1991; Seeber et al., 1995; Seeber, 2015) (c.f. Figure B3.6 and Chapter B3.3.5). The importance of superconducting grain boundaries for achieving high critical current densities in polycrystalline materials is discussed below. Detailed TEM has been performed on a range of bulk samples of $(Pb,Gd)Mo_6S_8$ and used to show that material can be produced with coherent tilt grain boundaries. Figure B3.7 shows some HREM demonstrating that in good material the grain boundaries are free of second phase. In some cases, dislocations are observed that occur at regular intervals along the boundary (Eastell, 1998). Detailed HREM on $Ni_2Mo_6S_8$ has shown that edge dislocations, which include an extra plane of Mo_6S_8 clusters, can form. Both coherent and incoherent interfaces have been found in this Ni-based compound (Kang et al., 1994). A small number of sulphur defects in the clusters were also observed (i.e. $Ni_2Mo_6S_{7.6}$). It has been several decades since small three-layer coils were fabricated using $PbMo_6S_8$ to demonstrate their potential use in magnet applications (Kubo et al., 1993), but the potential benefits of hot-drawing routes have garnered new interest in using Chevrel phase wires more recently (Seeber, 2015).

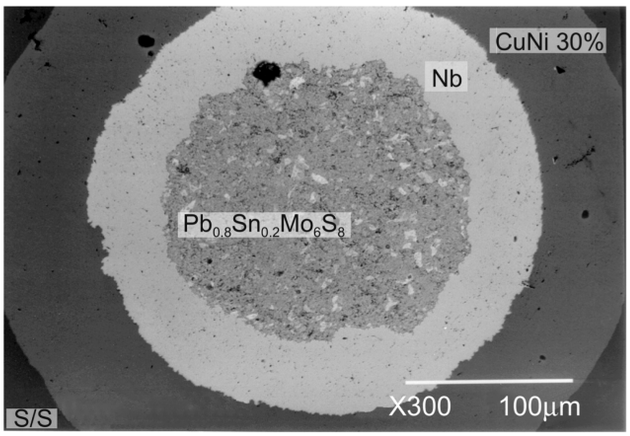

FIGURE B3.6 A $Pb_{0.6}Sn_{0.4}Mo_6S_8$ powder-route wire [measured in (Cheggour et al., 1997) and (Eastell, 1998)] which has a critical current density value of 6.7×10^8 A m^{-2} at 14 T and 4.2 K (Cheggour et al., 1998). The Nb is a diffusion barrier. The CuNi30% is a hard material that reduces damage to the Nb during drawing. The stainless steel (S/S) provides additional mechanical strength and precompresses the Chevrel phase core after cool down.

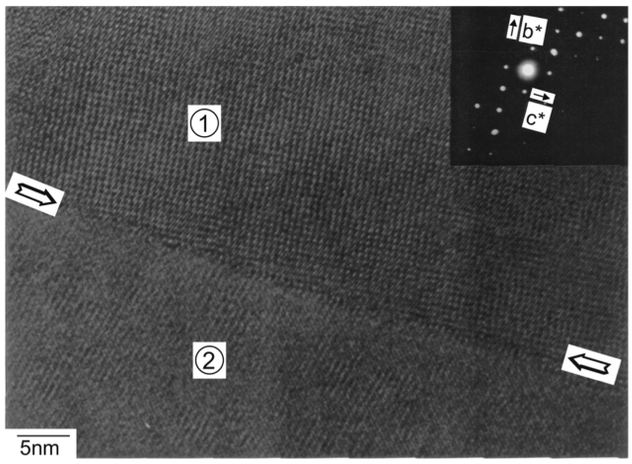

FIGURE B3.7 A high-resolution electron micrograph (HREM) of a grain boundary of $Pb_{0.7}Gd_{0.3}Mo_6S_8$ bulk sample. The selected area diffraction pattern (SADP) is for grain (1) and is close to the [100] zone axis. The grain boundary is very narrow (Eastell, 1998).

B3.4 Mechanical Properties

Among Chevrel phase materials, the coefficient of thermal expansion (α) has been studied most extensively for $PbMo_6S_8$. Using x-ray diffraction in the range 10 K–1200 K on bulk material, it has been concluded that α is almost temperature independent up to 900 K (650°C), where $\alpha = 1/L\ (dL/dT) = 9.4 \times 10^{-6}$ K^{-1} (Miraglia et al., 1987). For comparison, at room temperature α for $PbMo_6S_8$ is about half that of Cu or steel, about 25% higher than Nb and about twice that of Mo (Miraglia et al., 1987). Single-crystal measurements show a relatively strong anisotropic variation for α of about a factor of 3 (Alekseevskii et al., 1988). Such considerations are particularly important for optimising Chevrel phase wires (Miraglia et al., 1987). High-resolution thermal expansion measurements have been made using capacitive techniques. These show a very strong change in α at T_C in $PbMo_6S_8$ but not in $SnMo_6S_8$ (Ingle et al., 1998) which was attributed to different coupling between the superconductivity and the trigonal–triclinic structural transition (c.f. Chapter B3.3.5).

Compressibilities have been measured for 11 sulphur and selenide Chevrel phase compounds (Webb and Shelton, 1978) and typical data shown in Figure B3.8. The Young's modulus calculated from these data is around 40 GPa (Miraglia et al., 1987). This makes it similar to indium, about a factor of 5 smaller than steel and eight times smaller than Mo. Elastic constants have also been measured using ultrasonic techniques. The elastic constant for transverse distortions is 90 GPa and for longitudinal distortions is 21 GPa (Wolf et al., 1996).

The strain tolerance of Chevrel phase material has been investigated most comprehensively in the context of wires (Goldacker et al., 1989b). $PbMo_6S_8$ and $SnMo_6S_8$ fracture at about 0.65%, which is typical for a ceramic material.

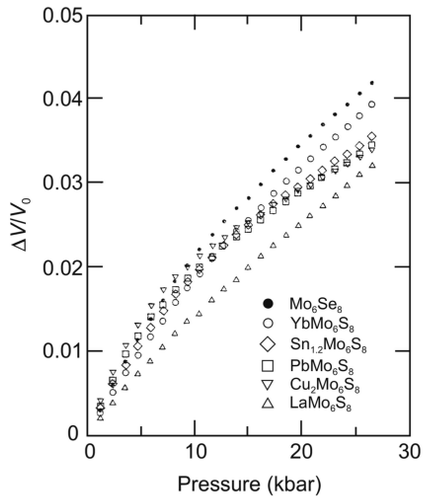

FIGURE B3.8 The compressibility of five ternary molybdenum sulphides $M_XMo_6S_8$ and the binary compound Mo_6Se_8 (Webb and Shelton, 1978).

Mechanical properties such as fracture toughness, crack propagation and fatigue properties are strongly dependent on the porosity of the material. Chevrel phase materials, therefore, can be considered as soft ceramics.

B3.5 Optical Properties

Vibrational Raman spectra have been observed for Cu-, Pb-, Ba- and Sn sulphide Chevrel phase compounds in the range from 10 meV to 50 meV (Holmgren et al., 1987) as shown in Figure B3.9. Such measurements give energies and symmetries

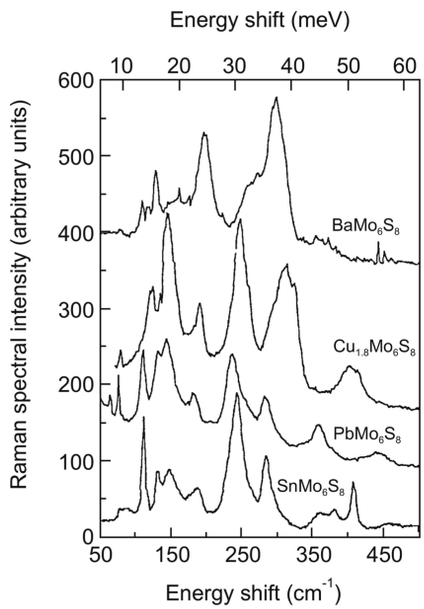

FIGURE B3.9 The Raman spectra for $BaMo_6S_8$, $Cu_{1.8}Mo_6S_8$, $PbMo_6S_8$ and $SnMo_6S_8$ (Holmgren et al., 1987).

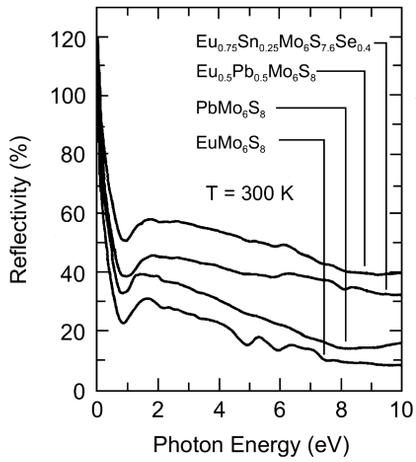

FIGURE B3.10 The near-normal reflectivity at room temperature of $EuMo_6S_8$, $PbMo_6S_8$, $Pb_{0.5}Eu_{0.5}Mo_6S_8$ and $Sn_{0.25}Eu_{0.75}Mo_6S_{7.6}Se_{0.4}$ (Fumagalli and Schoenes, 1991).

of the Raman active optical phonons near the Brillouin zero centre. Several bands or peaks are independent of the metal (M) atom even in the non-stoichiometric Cu-compounds, in broad agreement with tunnelling data (Ohtaki et al., 1984). Reflectivity measurements and complex magneto-optical Kerr-effect measurements have been completed in magnetic fields up to 12 T and temperatures down to 0.5 K (Fumagalli and Schoenes, 1991).

Figure B3.10 shows that the reflectivity (and optical conductivity spectra) are similar for $Eu_{1-x}Pb_xMo_6S_8$ and $Eu_{1-x}Sn_xMo_6S_{8-y}Se_y$ at 300 K. The carrier density was low ($\sim 6 \times 10^{27}$ m^{-3}), the mobility ~ 1 $cm^2\ V^{-1}\ s^{-1}$ and the effective masses for the carriers ~10 m_e (Fumagalli and Schoenes, 1991).

B3.6 Thermal Properties

The specific heat capacity (C_P) of $PbMo_6S_8$ has been measured by a number of authors in high magnetic fields up to 24 T (Cattani et al., 1988; Cors et al., 1990; van der Meulen et al., 1995). The electronic contribution in the normal state is ~7 mJ K^{-2} (g-at)$^{-1}$. In the superconducting state, in addition to the BCS exponential gap term, there is also the term linear in temperature that accounts for the normal cores of the fluxons in the mixed state. At the superconducting jump C/T is ~ 70 mJ K^{-2} (g-at)$^{-1}$, which is relatively high because of the soft modes present (Bader et al., 1976), and $\Delta C_e/T_C$ is about 12 mJ K^{-2} (g-at)$^{-1}$. The effective Debye temperature measured using C_P measurements changes by a factor of 2 from ~200 K at 4.2 K up to ~400 K at room temperature (Fradin et al., 1976).

Measurements and analysis of a large number of Chevrel-type superconductors have been completed (Lachal et al., 1984). Figure B3.11 shows a typical Debye plot for a series of compounds of the form $Pb_{1-x}Cu_{1.8x}Mo_6S_8$ (Niu et al., 2002). Ultrasonic measurements give an average Debye temperature of ~245 K (Wolf et al., 1996). Many magnetic Chevrel phase

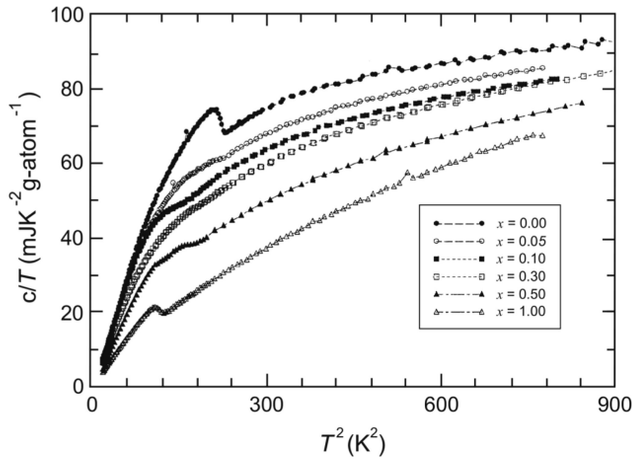

FIGURE B3.11 Debye plot (heat capacity)/(temperature) versus (temperature)^2 for $(Pb_{1-x}Cu_{1.8x})Mo_6S_8$ for different values of x (Niu et al., 2002).

superconductors have also been measured (Fischer and Maple, 1982a). Such work includes investigating pressure-induced reentrant superconductivity (Chen et al., 1993) and the reduction in $\Delta C_e/T_C$ with increased magnetic doping (Leigh, 2001). Nevertheless, there is typically a factor of 2 variation in all the parameters derived from specific heat data in the literature (N.B. for $PbMo_6S_8$, 1 mole = 1037 g = 15 gat.). The differences are attributed to the sensitivity of the materials to the fabrication process.

The consensus on the phonon density of states in Chevrel phase materials is good. The weighted phonon density of states for $PbMo_6S_8$ and $SnMo_6S_8$ measured using neutron scattering measurements and specific heat measurements is consistent with calculations that assume the Mo_6S_8 clusters are tightly bound but only weakly interact with other clusters or the M ion. There is a relatively flat dispersion curve and a strong peak at about 5 meV, associated with the Einstein mode from the M ion. Modes in the energy range up to 18 meV are associated with the soft external modes of the Mo_6S_8 clusters. The hard internal modes are responsible for the energy range from 18 meV to 50 meV (Bader et al., 1976).

B3.7 Normal-State Properties

The normal-state resistive properties of Chevrel phase compounds are rather well described in terms of their chemistry and are consistent with band structure calculations (Mattheis and Fong, 1977). The dominant carriers are holes associated with the $4d_{x2-y2}$ states. The three important factors that contribute to the electronic properties are the charge transfer from the M cation to the Mo_6S_8 cluster and the volume and structure of the unit cell.

The position of the Fermi level in the sulphide system is strongly related to the charge transfer between the M cations and the sulphur anions (Yvon and Paoli, 1977). A characteristic of the Mo_6S_8 cluster is that it is only slightly distorted when filled with 24 electrons and tends to be insulating. The electronic configuration of $Mo4d^55s^1$ contributes six electrons to the Mo_6S_8 cluster. Hence with the S in the –2 valence state, there are 20 electrons in the Mo_6S_8 cluster and there is hole conduction. Adding Pb or Sn to the structure (both have valence +2) increases the number of electrons to 22, equivalent to two holes per cluster which produces the highest value of T_C. For comparison, the valence of the S, Se and Te in Mo_6S_8, Mo_6Se_8 and Mo_6Te_8 are –2, –1.75 and –1.33, respectively. Band structure calculations show that in the rhombohedral $PbMo_6S_8$, the Fermi energy lies below an energy gap about 1 eV wide (Mattheis and Fong, 1977). The states near to the Fermi energy are strongly confined within the Mo_6S_8 cluster (Bullett, 1977). Indeed there are some broad similarities between Chevrel phase materials and the intercalates of TaS_2 (Prober et al., 1980) and MoS_2 (Woollam and Somoano, 1976), where there is a hybridisation of the metal d-bands and an associated energy gap (Mattheis, 1973). The band structures for the Chevrel phase selenides and the telluride have similar properties (Bullett, 1977) (Roche et al., 1999), but one of the marked differences between them and the sulphides is that the density of states at the Fermi energy is higher for trivalent ions than for divalent ions. This is supported by the T_C values which are higher for the rare-earth selenides than for the sulphides as shown in Figure B3.1.

In $PbMo_6S_8$ samples, the resistivity (ρ) at room temperature is about 100 μΩ cm–1 mΩ cm, and typical values for room temperature–resistivity ratio (RRR) are 4 to 6 (Miraglia et al., 1987; Niu et al., 2002). In the $Cu_xMo_6S_8$ single crystals, ρ is similar with a RRR value of about 7 which leads to a scattering length (l) of about 20–30 Å (Fischer and Maple, 1982a). In thin films, RRR values were found in the range 2–6 and l estimated to be ~40 Å (Alterovitz and Woolam, 1978). The temperature dependence of ρ(T) is approximately linear up to 50 K but shows negative curvature at higher temperatures similar to the A15 superconductors. Theories that address the non-linearity utilise a strong peak in the density of states (Cohen et al., 1967) or a scattering length that is comparable to the lattice spacing (Fisk and Webb, 1976; Sunandana, 1979). Experimental data at low temperatures can be misleading, particularly if the material includes pure Mo or Mo_2S_3. Hall effect measurements in the $(Eu_{1-x})Sn_xMo_6S_8$ at room temperature gives Hall coefficients of $+0.7 \times 10^{-3}$ cm^3 G^{-1} confirming a hole carrier concentration of $\sim 9 \times 10^{27}$ m^{-3} (Meul, 1986) [in agreement with the optical measurements and muon measurements (Birrer et al., 1993)] and implying ~2.5 holes per formula unit. In $REMo_6S_8$ compounds, ρ is typically ~300 μΩ cm and RRR range from 8 to 34 (Beille et al., 1991), although $LuMo_6S_8$ has a resistivity at room temperature of only 50 μΩ cm (Geantet et al., 1990). Limited thermopower measurements on $Cu_{1.8}Mo_6S_{8-x}Te_x$ have also been completed (Kaiser, 1997).

The density of states derived from susceptibility measurements, specific heat measurements and band structure calculations give consistent values. For the Pb- and Sn Chevrel

phase sulphide compounds, χ is about 3.5×10^{-5} emu (g-at)$^{-1}$. The (phonon-enhanced) density of states calculated from C_p measurements is about 1 state per (eV-atom-spin). This is about twice that found from χ measurements or band structure calculations which is expected with strong electron–phonon coupling (Fischer, 1978). In materials with relatively high critical temperature $PbMo_6S_8$, $LaMo_6S_8$ and $LaMo_6Se_8$, the susceptibility varies by about a factor of 1.5–2 between room temperature and 20 K (Peña and Sergent, 1989; Peña et al., 1998) and shows an anisotropy (for single crystals) of ~40%. A strongly temperature-dependent susceptibility has also been observed in the high-temperature superconductors. This is taken to be evidence that the Fermi level is situated near a peak in the density of states which standard BCS theory (Bardeen et al., 1957; Abrikosov, 2000) associates with relatively high-T_C values.

B3.8 Superconducting Properties

B3.8.1 Transition Temperature

The BCS theory (Bardeen et al., 1957; Abrikosov, 2000) currently provides the only generally accepted microscopic explanation for superconductivity. Within this framework, the critical temperature is determined by the density of states at the Fermi level, the phonon spectrum and the electron–phonon coupling. Tunnelling measurements on $Cu_{1.8}Mo_6S_8$ and $PbMo_6S_8$ give the ratio of the gap (Δ) to T_C of $2\Delta / k_B T_C = 4-5$ (BCS theory predicts 3.5) showing strong coupling. In the pseudobinary $Mo_6Se_{8-x}S_x$ system, strong coupling in Mo_6Se_8 (T_C = 6.2 K, coupling constant: λ = 1.25, $2\Delta / k_B T_C = 4.2$, $\Delta C_E / C_E = 2.25$) gives way to weak coupling showing BCS behaviour in $Mo_6Se_4S_4$ ($T_C = 1.8\ K$, λ = 0.6, $\Delta C_E / C_E = 1.4$) (Pobell et al., 1982; Furuyama et al., 1989). Although most of the phonon modes associated with the Mo_6S_8 cluster modes contribute to the electron coupling (Poppe and Wuhl, 1981), the materials with higher T_C values approaching 16 K have large values of λ, which are probably most strongly affected by the soft modes (Furuyama et al., 1989). Recent tunnelling spectroscopy provides evidence for two-gap superconductivity in both $PbMo_6S_8$ and $SnMo_6S_8$ (Dubois et al., 2007; Petrovic et al., 2011). The pseudobinary $Mo_6S_6I_2$ compound has the relatively high T_C of 14 K, which suggests that the superconductivity in Chevrel phases of highest T_C is fundamentally associated with the clusters. In this context, the isotope effect observed in Mo_6Se_8 is consistent with BCS theory and suggests that an electron–phonon mechanism operates in Chevrel phase materials (Pobell et al., 1982). For a given structure, T_C also depends on the volume of the unit cell (Hinks et al., 1984) and the valence electron concentration in the Mo_6S_8 cluster (Sergent et al., 1978). The trivalent sulphur-based Chevrel phase materials have uniformly low T_C whereas the divalent trigonal materials have high T_C (e.g. Sn and Pb). Among the trivalent rare-earth ions, there is a correlation between T_C and the volume of the unit cell (Fischer, 1978). When the volume decreases, the intercluster Mo–Mo decreases, so the valence bands are expected to broaden, and the density of states and T_C to fall (Fischer et al., 1975a). Hydrostatic pressure has been used to change the volume of the unit cell, and hence T_C, in divalent sulphides (Shelton, 1976; Capone II et al., 1984; Hinks et al., 1984). The effect of pressure on T_C is about an order of magnitude higher than found in elemental superconductors (Shelton, 1976) $dT_C / dP \sim 10^{-4}$ (kbar)$^{-1}$. The difference in critical temperature (T_C) between $PbMo_6S_8$ and $SnMo_6S_8$ can be explained by the difference in the volume of the unit cell (Hinks et al., 1984).

The Chevrel phase materials that transform fully from a rhombohedral structure at high temperatures to a triclinic structure at low temperatures have low electronic density of states (Lachal et al., 1983) and are non-superconducting. However, the superconductivity can be restored if pressure is applied to prevent the triclinic transition occurring. In $BaMo_6S_8$ for example, applying a pressure of 4 GPa changes the material from a triclinic semiconductor to a mixed triclinic–rhombohedral phase that is metallic with a T_C of 12 K (Yao et al., 1988). The structural instabilities in the Chevrel phase superconductors may enhance the electron–phonon coupling. In $Eu_{1.2}Mo_6S_8$ (Chu et al., 1981), (shown in Figure B3.12) superconductivity is also close to the metal–insulator transition and can be tuned by pressure. In $(Sn_{1-x}Eu_xM)_{1.2}Mo_6S_8$ (Harrison et al., 1981), the transition is tuned by Sn content (or carrier concentration). These properties are found in other Chevrel phase materials and is reminiscent of the HTS materials where high–T_C values also occur in materials with relatively low carrier concentration that are in proximity to the metal–insulator transition. There has been intense research into alternative

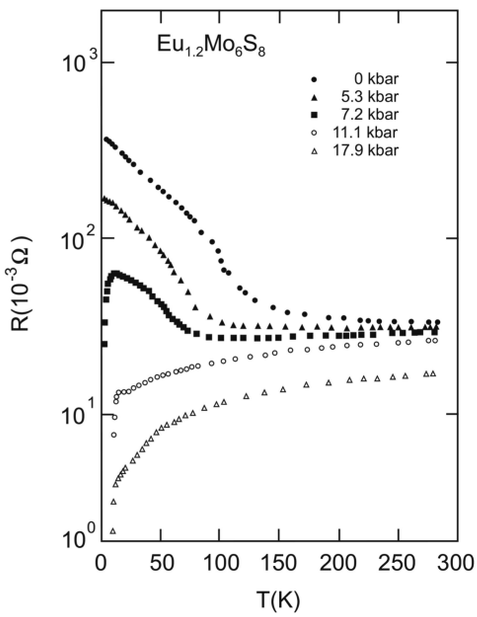

FIGURE B3.12 The resistance versus temperature for $Eu_{1.2}Mo_6S_8$ at various pressures (Chu et al., 1981).

microscopic mechanisms for superconductivity following the discovery of the high-temperature superconductors in the late 1980's. The Uemura plot provides empirical evidence that the cuprate and bismuthate high-temperature superconductors, the organic, Chevrel phase and heavy Fermion systems all belong to a single class of superconductors where T_C is proportional to the (small) n_s/m^* (carrier density/effective mass) (Uemura et al., 1991; Harshman and Mills Jr, 1992; Uemura, 2004) as shown in Figure B3.13. In the cuprates, the high values of T_C and the lack of a clear isotope effect suggest a non-phononic mechanism (Batlogg et al., 1987). For Chevrel phase materials, the carrier density ($n_s \sim 2$ holes/unit cell) and the effective mass ($m^* \sim m_e$) are rather robust numbers from both experiment and theory. Their presence on the Uemura plot suggests that Chevrel phase materials, which have a well-known chemistry and electronic structure, may be model systems in which to investigate non-standard mechanisms for superconductivity because of the simplifications which follow from their (almost) cubic (isotropic) structure.

The simple proportionality and universal behaviour in Figure B3.13 provides evidence that a single mechanism may produce superconductivity in many different types of superconductors including the Chevrel phase materials (Hillier and Cywinski, 1997; Sonier et al., 2000; Kiefl et al., 2010). Given that over the last 20 years, most classes of new superconductors appear close to the Universal line in the Uemura plot, it no longer makes much sense to describe them as exotic superconductors or high-temperature superconductors. Nevertheless, the plot does provide a guide as to how to synthesize materials with even higher T_C (Rybicki et al., 2016) and insight into the underlying canvas or phase diagram for the microscopic details for these materials (Uemura, 2009). Also, it naturally opens the questions of how the electrons pair to form bosons and whether the bosons are first preformed and then condense at T_C (in a similar way to superfluid helium) (Dzhumanov et al., 2016). Without a microscopic theory, we don't know whether the temperature at which bosons may preform bears any relation at all to the temperature at which superconductivity appears (c.f. Figure B3.14). Alternatively, akin to the BCS model, the electrons may become pairs and condense at the same temperature. One of the central issues remains the signature linear temperature dependence found for the normal-state resistivity of 'non-BCS' superconductive materials up to temperatures well above the Mott metal–insulator transition temperature (Gurvitch and Fiory, 1987) which has led to the 'strange metal' notation. Some authors associate the strange metal and the superconductivity (Loram et al., 2001; Tallon and Loram, 2001) with the quantum critical point. Others suggest that the pseudogap competes with the superconductivity (Kondo et al., 2009) or that the strange metal behaviour can be explained without any 'exotica' such as the quantum critical point (Anderson, 2006). Were a single mechanism able to explain the Universal superconductivity behaviour in the Uemura plot, it would clearly simplify things. Unfortunately identifying such commonality is not straightforward since even in a single material there are contradictory results reported. For example in Bi-2212, some authors report pseudogap behaviour only in underdoped samples (Ding et al., 1996; Williams et al., 1997; DeWilde et al., 1998), some that T^*

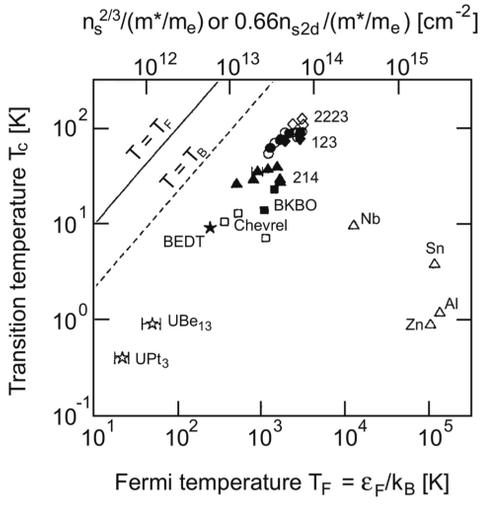

FIGURE B3.13 An Uemura plot – a log–log plot of critical temperature (T_C) versus the Fermi temperature (T_F) estimated from muon spin resonance measurements (combined with the interplanar distance for 2D and the Sommerfeld constant for 3D systems) for Cuprates, BKBO, Chevrel phase, BEDT, heavy fermion and some elemental superconductors. The solid line and the dashed line show when the critical temperature equals the Fermi temperature, T_F, and the dashed line represents the Bose–Einstein condensation temperature, T_B, of the ideal boson gas versus the (Uemura et al., 1991; Uemura, 2004).

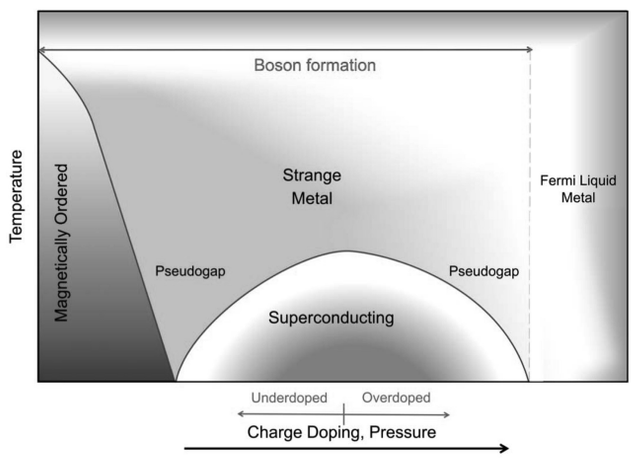

FIGURE B3.14 A schematic phase diagram for a Bose–Einstein type of condensation mechanism for superconductivity that occurs near the metal–insulator transition in metals with low carrier density. In the conducting phase, over a range of carrier concentration, the bosons are preformed at higher temperatures and eventually condense into the superconducting phase.

just gives the temperature scale of the pseudogap (Williams et al., 1997), and others that the same generic tunnelling density of states, or pseudogap behaviour, occurs in both overdoped and underdoped materials (Renner et al., 1998). Although the microscopic mechanism for superconductivity in the Chevrel phase materials has long been considered to be classic BCS because of the isotope effect found in $Mo_6Se_{8,}$ and the reasonable agreement between microscopic normal-state properties and the predictions of BCS theory for T_C, Figure 13 shows that there is some important microscopic Physics that we just have not discovered yet – an understanding that will explain why superconductors appear together on the Uemura plot. Our current understanding is not complete. Indeed some authors have even argued that the simple empirical proportionality shown in Figure B3.13 does not hold in Chevrel phase materials (Birrer et al., 1993) but is best described using a rather more complex percolation model dependence (Dallacasa and Feduzi, 1992). We conclude that we just do not know yet whether we should classify Chevrel phase materials as classic BCS or non-BCS superconductors (Hirsch et al., 2015a; Hampshire, 2020).

B3.8.2 Upper Critical Field

Given that the only microscopic theory available to the community is BCS theory (Bardeen et al., 1957; Abrikosov, 2000), and so a large body of research has been described using it, we state here that the upper critical field (B_{C2}) can be given by:

$$\boldsymbol{B}_{C2}(0)=\left(8.3\times10^{34}\left[\frac{\gamma \boldsymbol{T}_C}{\boldsymbol{S}}\right]^2+3.1\times10^{3}\gamma\rho_N\boldsymbol{T}_C\right) \qquad \text{(B3.1)}$$

where the two terms are the clean and dirty contribution, respectively (Decroux et al., 1993; Morley et al., 2001) and are consistent with $\xi_0 \sim l$. Both terms contribute to the very high upper critical field values in the $PbMo_6S_8$ and $SnMo_6S_8$ compounds. The complexity of the intrinsic spin, orbital coupling and spin-orbit coupling must also be included, using Werthamer–Helfand–Hohenberg (WHH) theory, to describe the temperature dependence of $B_{C2}(T)$ (Werthamer et al., 1966). However, further theoretical work is still required to assess whether the parameters derived are physically significant. The anisotropy of B_{C2} in $PbMo_6S_8$, $PbMo_6Se_8$ $Cu_{1.8}Mo_6S_8$ and $SnMo_6Se_8$ has been found experimentally to be about 15% (Decroux et al., 1978; Decroux and Fischer, 1982; Pazol et al., 1989) (as shown in Figure B3.15) and correlated with the rhombohedral angle (c.f. Chapter B3.3.5). There is currently no adequate explanation for this, since the band structure calculations show nearly cubic symmetry and predict low anisotropy.

B3.8.3 Ginzburg–Landau Description

Ginzburg–Landau (G–L) theory provides a self-consistent explanation for the properties of metallic superconductors in-field (i.e. superconductors that are non-magnetic in the normal state). There are only two free parameters, which can be taken to be the G–L constant (κ), which is broadly temperature independent, and $B_{C2}(T)$ (Cave, 1998). The fundamental properties of the superconducting state can be determined by measuring the reversible magnetisation close to $B_{C2}$and using the G–L relation:

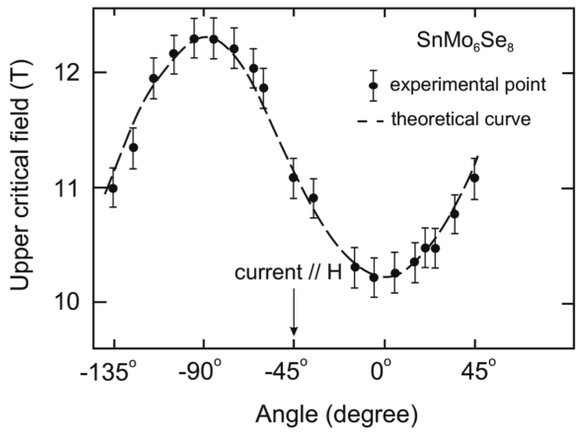

FIGURE B3.15 The anisotropy of the upper critical field of $SnMo_6S_8$ at 4.2 K (Decroux et al., 1978). The angle is measured between the ternary axis and the magnetic field.

$$\boldsymbol{M}=-\left(\frac{\boldsymbol{H}_{C2}-\boldsymbol{H}}{\left(2\kappa^2-1\right)\beta_A}\right) \qquad \text{(B3.2)}$$

where H_{C2} is the critical field strength, H is the applied field strength and β_A (≈ 1.16) is the Abrikosov constant (Kleiner et al., 1964). Reversible magnetisation measurements similar to those shown in Figure B3.16 can be used to obtain values for κ and $dB_{C2}(T)/dT$, from which the slopes $dB_C(T)/dT$ and $dB_{C1}(T)/dT$ can be calculated. For high κ materials such as

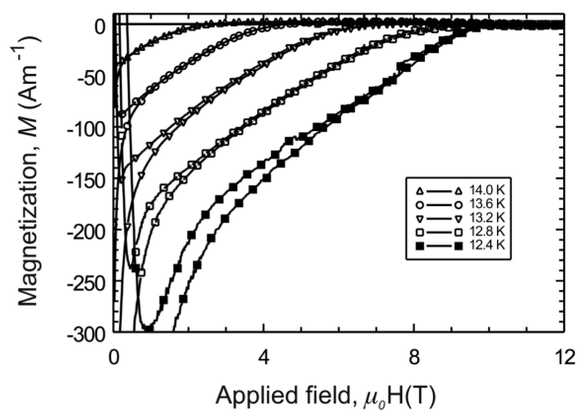

FIGURE B3.16 The magnetisation of bulk $PbMo_6S_8$ as a function of field at different temperatures. From the reversible data, one can use Ginzburg–Landau theory to calculate the Ginzburg–Landau parameter and the upper critical field (Zheng et al., 1995; Niu et al., 2002).

TABLE B3.3 The Values of the Fundamental Superconducting Parameters of $PbMo_6S_8$ Derived from Reversible Magnetisation Data (Zheng et al., 1995)[a].

T_C	κ	$B_{C2}(0)$	$B_{C1}(0)$	$B_C(0)$	$\lambda_{GL}(0)$	$\xi_{GL}(0)$
13.7 K	130	56 T	6.4 mT	250 mT	230 nm	2.0 nm

[a] The *h*, *k* and *l* values are provided for the hexagonal structure.

the Chevrel phase superconductors, it is best not to calculate the critical fields at low temperatures using the G–L relations directly, since G–L theory is strictly only valid close to T_C. In order to calculate $B_{C2}(0)$, the WHH relation can be used where:

$$B_{C2}(0) = -0.7T_C \left.\frac{dB_{C2}}{dT}\right|_{T_C} \tag{B3.3}$$

$B_C(0)$ can be calculated using the BCS expression

$$B_C(T) = 1.74B_C(0)\left(1-\frac{T}{T_C}\right) \tag{B3.4}$$

and $B_{C1}(0)$ can be calculated using the Gorter–Casimir (Gorter and Casimir, 1934) two-fluid empirical relation:

$$B_{C1}(T) = B_{C1}(0)\left(1-\left(\frac{T}{T_C}\right)^2\right) \tag{B3.5}$$

Note that this approach does mean that the G–L relations do not hold at low temperatures (Zheng et al., 1995) – for example $B_{C2}(0) \neq \varphi_0 / 2\pi\xi^2_{G-L}(0)$. However, more reliable values for the critical fields are found at low temperatures using this procedure. The critical parameters for $PbMo_6S_8$ are shown in Table B3.3. The penetration depth has been measured in $SnMo_6S_{8-x}Se_x$ and $PbMo_6S_{8-x}Se_x$ (Birrer et al., 1993) using both magnetic and muon measurements and reasonably good agreement found.

B3.8.4 Irreversibility Field

The concept of the irreversibility field (B_{IRR}) is well documented in the literature both in the high-temperature and low-temperature superconductors (Rossel et al., 1991; Youwen and Suenaga, 1991). B_{IRR} is the magnetic field (below B_{C2}) at which the critical current density falls to zero. An important experimental problem is that measurements can only determine the field at which J_C drops below a minimum detection level. For practical purposes, a number of techniques are used, although the best procedure to measure B_{IRR} has not been generally agreed.

Vibrating sample magnetometry (VSM) can determine the field which delineates the hysteretic and reversible magnetic properties of a material and hence B_{IRR} directly (Cave, 1998). Such measurements have been performed on $PbMo_6S_8$. In bulk $PbMo_6S_8$, it was found that $B_{IRR} = 63(1-T/T_C)^{1.46}$ (Zheng et al., 1995). A similar power law has been observed in single crystals (Rossel et al., 1991) and derived theoretically using a thermally activated flux-creep model (Yeshurun and Malozemoff, 1988). Measurements have also been completed on $(Pb_{1-x}Gd_x)Mo_6S_8$ that demonstrate B_{IRR} decreased with increased Gd content (Zheng and Hampshire, 1997). However, one should be very careful interpreting such data, since the hysteresis in magnetisation found in VSM measurements can only be simply related to J_C using Bean's model (Bean, 1962) if the field applied to the sample is uniform (c.f. Figures B3.17 and B3.18). Consider a typical material in which J_C reduces as the applied magnetic field increases and approaches B_{c2}. In general, the hysteresis collapses to zero when the variation in applied field

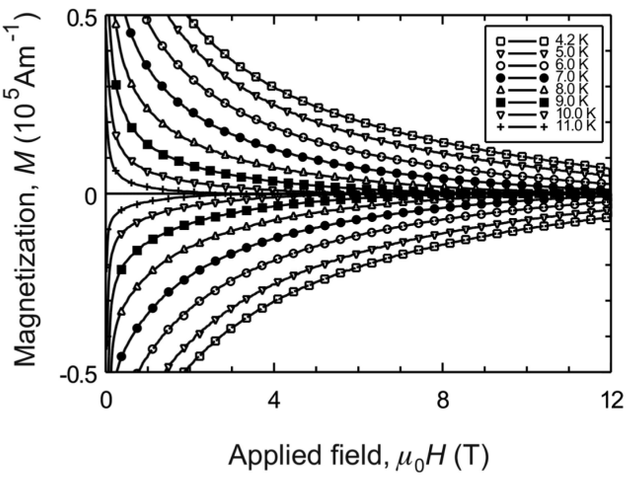

FIGURE B3.17 The magnetisation of bulk $PbMo_6S_8$ as a function of field at different temperatures (Niu et al., 2002). From the magnitude of the hysteresis, one can calculate the critical current density using Bean's model (Bean, 1962).

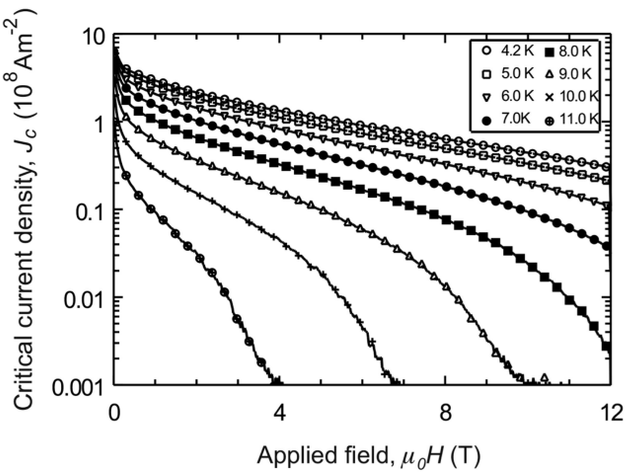

FIGURE B3.18 The critical current density of bulk $PbMo_6S_8$ as a function of field at different temperatures calculated using the data from the magnetisation data in Figure B3.17 and Bean's critical state model (Niu et al., 2002).

the sample experiences while oscillating is equal to the self-field of the sample and not when J_C is zero. For example in Figure B3.16, although the hysteresis falls dramatically at 12.8 K when the applied field reaches 0.5 T, it is associated with the inhomogeneity of the applied field and not related to B_{IRR} at all (Daniel and Hampshire, 2000). In such cases, any comparison of such field values with theoretical calculations of B_{IRR} is compromised, although one can say that the comparisons are useful to assess practical limits for high-field applications.

Flux penetration measurements and transport measurements offer alternative means to measure the critical current density (Ramsbottom and Hampshire, 1999). A type of irreversibility field can be determined by extrapolating the functional form of J_C to zero using a Kramer extrapolation (Kramer, 1973). In $PbMo_6S_8$, the irreversibility field has been improved from ~22 T up to nearly 40 T at 4.2 K by fabricating the material using hot isostatic pressing (Ramsbottom and Hampshire, 1997). B_{IRR} values of 35.4 T at 4.2 K have been achieved in high J_C (Pb,Sn)Mo_6S_8 wires (Cheggour et al., 1998). Standard resistance or susceptibility measurements can also be used to determine B_{IRR} (Nakamura et al., 1997). However, values obtained using different techniques can differ markedly. For example, increasing the Gd content in (Pb,Gd)Mo_6S_8 increases the irreversibility field in high fields measured using the onset of the resistive transition but shows a decrease using the onset of the susceptibility transition (Ramsbottom and Hampshire, 1999).

B3.8.5 Pinning Energy

The apparent pinning energy (U*) of $PbMo_6S_8$ has been measured using the decay of the magnetisation in time (Zheng et al., 1995). U* is calculated to vary from about 40 meV at 2 T to 15 meV at 12 T at 4.2 K. These values are about double the equivalent values found in $YBa_2Cu_3O_7$ and four times that of $Tl_2Ba_2Ca_2Cu_30_{10}$ at low fields. Activation energies derived from Arrhenius plots of resistivity give 130 meV at 9 T for $PbMo_6S_8$ and 186 meV at 9 T and 4.2 K for $SnMo_6S_8$ (Gupta et al., 1994). Comparisons between equivalent measurement techniques suggest that the effect of 'flux creep' is more pronounced in $PbMo_6S_8$ than in NbTi but less than that in high-temperature superconductors.

B3.8.6 Microwave Surface Resistance

Very few microwave measurements have been completed on Chevrel phase superconductors. For a superconducting $Cu_2Mo_6S_8$ thin film, a surface resistance of 4.5 mΩ at 10 GHz and 4.2 K has been obtained (Lemee et al., 1998).

B3.8.7 Critical Current Versus Field and Temperature

The mechanism that determines the critical current density has long been a topic of theoretical and experimental research. J_C is determined both by the intrinsic fundamental superconducting properties and by the extrinsic metallurgical and microstructural factors such as the grain size of the material. Fietz and Webb (Fietz and Webb, 1967) suggested parameterising J_C through a scaling law for the volume pinning force ($F_P = J_C \times B$). The Chevrel phase materials can be described using

$$\boldsymbol{F_P = J_C \times B = \propto \left(B^*_{C2}(T)\right)^n b^{\frac{1}{2}}(1-b)^2} \qquad \text{(B3.6)}$$

where $B^*_{C2}(T)$ is the effective upper critical field, α and n are constants and b is the reduced field ($B/B^*_{C2}(T)$) (Cheggour et al., 1998). The index n is typically between 2 and 3 as found in many A15 materials (Keys et al., 1999; Keys and Hampshire, 2003; Taylor and Hampshire, 2005).

In low fields, the parameter α increases as the grain size decreases as is also found in low-temperature superconductors such as Nb_3Sn (Schauer and Schelb, 1981). There are many different approaches to modelling the pinning including that of Kramer after whom the reduced field dependence is named but which is probably not correct in detail (Kramer, 1973; Hampshire et al., 1985). Other pinning models have also been suggested that give the Kramer dependence and emphasise the importance of the grain boundaries. As yet, however, there is no consensus on the nature of the pinning that causes the ubiquitous Kramer dependence (Dew-Hughes, 1974; Hampshire and Jones, 1987; Gupta et al., 1994).

In materials optimised for high J_C in high fields, there is a much weaker correlation between J_C and grain size. For example, at 4.2 K in $SnMo_6S_8$, J_C is almost independent of grain size at fields above 15 T (Bonney et al., 1995). In $PbMo_6S_8$, it has been reported that J_C at 6 T saturates for grain sizes below 0.3 μm, although it must be noted that these samples are not fully dense (Karasik et al., 1985). Kramer found a similar saturation (or peak effect) close to B_{C2} in many low-temperature superconductors (Kramer, 1975; Daniel et al., 1997). The value of field at which J_C extrapolates to zero ($B^*_{C2}(T)$) is strongly correlated with the properties of the grain boundaries rather than either intragranular properties or the thermodynamic upper critical field (Cattani et al., 1991). Hence for high J_C materials, the standard grain boundary description may not be appropriate in the high-field (or saturation) regime. Whether this is because the efficiency of the grain boundaries falls or because a different [pinning (Le Lay et al., 1991; Gupta et al., 1994) or non-pinning (Hampshire, 1998)] mechanism limits J_C remains unresolved.

There has long been evidence that during dissipation (above J_C) flux flow in Chevrel phase materials can be localised along narrow channels (Herrmann et al., 1992). More recent experimental and (time-dependent Ginzburg–Landau) computational work has shown that the degradation of some critical properties at grain boundaries leads to a Kramer dependence for the volume pinning force. In such materials, flux penetrates the interior of a polycrystalline superconductor by first flowing along grain boundaries (Carty and Hampshire,

2008). This approach has opened the possibility that a general description of dissipation in many high-field polycrystalline superconductors is flux flow along grain boundaries (Carty and Hampshire, 2008, 2013; Sunwong et al., 2013).

The influence of neutron irradiation on J_C of Chevrel phase compounds has been investigated and some limited improvements were found (Rossel and Fischer, 1984). The highest J_C in wires is found in the quaternary (Pb,Sn)Mo_6S_8 for which at 4.2 K and 14 T, J_C is 7×10^8 A m^{-2} (Cheggour et al., 1997; Cheggour et al., 1998) and at 20 T about 2×10^8 A m^{-2} (Rimikis et al., 1991). Although the Pb-based Chevrel phase material has the highest critical field, some Sn is often included in bulk materials. This addition improves the homogeneity of the bulk (Selvam et al., 1995) and the interconnectivity between the grains probably by suppressing formation of MoS_2 (Even-Boudjada et al., 1999). Further improvements in the grain boundaries are still required to increase J_C.

A maximum value of J_C for $PbMo_6S_8$ has been estimated at 10^{10} A m^{-2} at 4.2 K and 20 T using a model which assumes ideal arrangement of the pinning sites (Rossel et al., 1991). Flux penetration measurements with small AC fields have found that $J_C > 10^{10}$ A m^{-2} at 4.2 K and 5 T at the surface of bulk $PbMo_6S_8$ which demonstrates the potential of this material (Kajiyana et al., 1985). Very significant improvements in J_C have been achieved in the upper critical field in Chevrel phase materials (Hampshire and Niu, 2005) by making it nanocrystalline which suggest we are far from optimum properties for polycrystalline materials. Along with most high-field polycrystalline superconductors, J_C in Chevrel phase materials is typically three orders of magnitude lower than its depairing current density (Wang et al., 2017) which leaves open the possibility of improvements – for example, following those of high-temperature superconductors, by fabricating highly textured (or single-crystalline) Chevrel phase material (Grant, 1995) and adding localised artificial pinning sites.

To produce magnetic fields above 25 T using superconductors alone requires rapid quench detection to protect the magnet from burn-out. This usually means that good magnet protection requires that the superconductor becomes as resistive as possible once it is outside its operating temperature range and a quench has occurred. Rapid quench detection is currently a problem for some HTS materials because the superconductor does not become resistive until it has been heated for a comparatively long time. This may be solved using better detection systems (Scurty et al., 2016), but if not, Chevrel phase materials may become attractive for quench control in magnet systems because of their relatively low-T_C values.

B3.9 The Magnetic Chevrel Phase Superconductors

Very small amounts of magnetic impurities at the parts-per-million level or paramagnetic ions at the 1 at% level are known to destroy the superconducting properties of most superconductors. Ginzburg observed that among the elements of the periodic table, superconductivity and magnetism seem to be mutually exclusive (Ginzburg, 1957) although clearly with the development of the Fe pnictide superconductors this observation is not generally true for complex compounds (Kamihara et al., 2008). Early experimental work investigating superconductors with magnetic impurities was compromised by uncertainty over whether or not the superconductivity and the ferromagnetism coexisted in the same region of the sample. Along with Chevrel phase superconductors, there are several other classes of superconductor that have magnetic ions within the superconducting unit cell. It is important in surveying this literature to distinguish magnetic order within the conducting layer and magnetic order produced by say magnetic rare-earth ions that hardly overlap with the conduction electrons/holes. The structure of magnetic Chevrel phase superconductors locates the rare-earth element a relatively large distance from the Mo atoms. This leads to a weak overlap between the 4d-electrons of the Mo and the 4f-electrons of the rare-earth element. This is similar to the cuprates where the rare-earth ions also hardly overlap with the conducting carriers. In contrast, the 3d-elements in Chevrel phase materials are located close to the Mo_6S_8 cluster, and the superconductivity is destroyed.

Susceptibility measurements show that the ternary magnetic superconductors with rare-earth elements have an effective Bohr magneton number that is close to the theoretical values for isolated ions at temperature above about 50 K (Johnston and Shelton, 1977; Pellizone et al., 1977). At lower temperatures, deviations from the Curie–Weiss law occur because of crystal field and magnetic correlation effects. There are many similarities in the superconducting and magnetic properties of the rare-earth Chevrel phase materials and the strongly magnetic nickel–boron–carbide materials (Eisaki et al., 1994), the rare earth–rhodium–borides and the cuprates because of the potential for the spatial separation of the rare-earth ions and the superelectrons. However, consider the properties of $GdMo_6S_8$ shown in Figure B3.19 (Fischer and Maple, 1982a) (Ishikawa et al., 1982). The re-entrant resistance is correlated with the antiferromagnetic ordering which occurs at 0.82 K as shown by the heat capacity measurements and neutron scattering measurements (Majkrzak et al., 1979; Thomlinson et al., 1981). The nature of the magnetic ordering is dependent on the particular rare-earth element in the compound and can be antiferromagnetic, ferromagnetic or oscillatory. For example in $HoMo_6S_8$, tunnelling spectroscopy suggests that superconductivity coexists with ferromagnetism (Morales et al., 1996). In high fields, so called re-entrant superconductivity can occur in some systems (Hampshire, 2001). It has been suggested that in high fields, the applied external field compensates for the negative exchange interaction between the rare-earth ion and the conduction electrons so that the material becomes superconducting (Jaccarino and Peter, 1962) in a limited part of B–T phase space. The degree to which ordering of the ions is exchange driven (Blount and

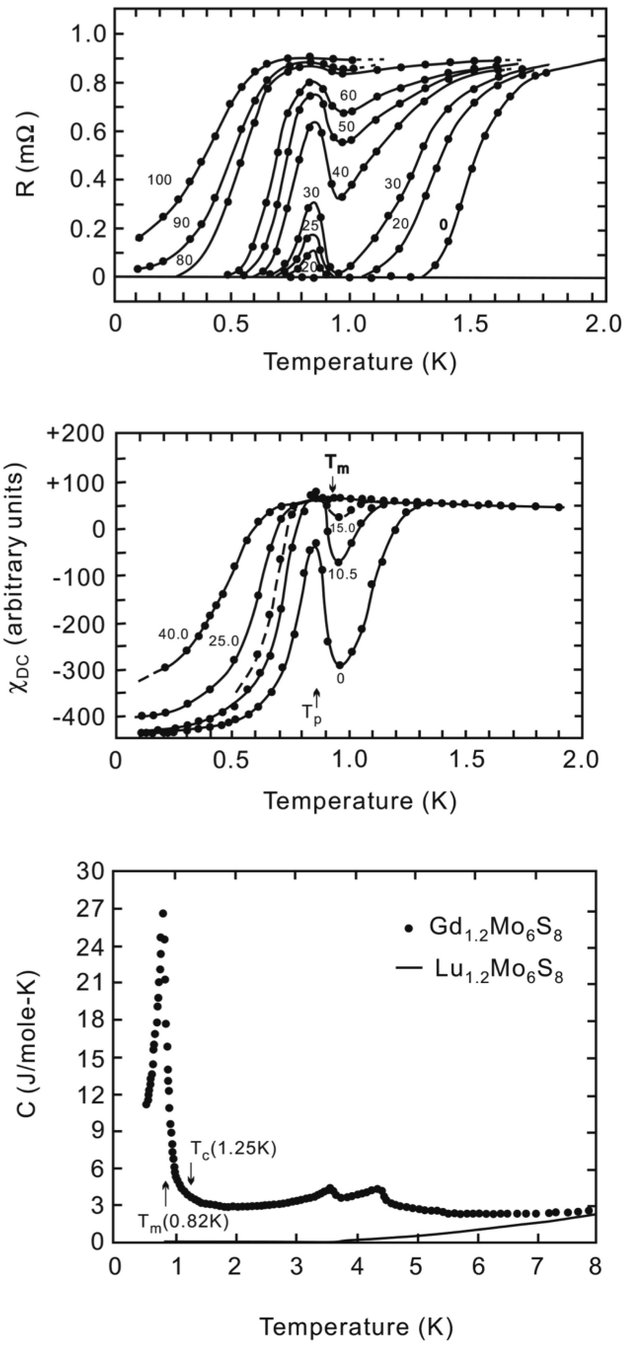

FIGURE B3.19 Selected properties of the magnetic rare-earth compound $GdMo_6S_8$ (Ishikawa et al., 1982).

Varma, 1979) and driven by dipolar interactions (Hampshire, 2001) is still open to discussion.

The range of phenomena of the rare-earth Chevrel phase superconductors continues to fascinate the scientific community. The complexity arises because in order to understand the properties of these materials we must understand how magnetism and superconductivity operate at the atomic level.

B3.10 Concluding Comments

Since their discovery in 1971, Chevrel phase materials have been of interest to the whole superconductivity community from engineers, who want to make high-field magnets, to physicists, who want to understand the microscopic mechanism that causes superconductivity, magnetism and coexistence of the two. Interest in these materials inevitably waned with the discovery of the high-temperature cuprate superconductors. Massive interest in HTS materials was driven by the possibility of discovering a new mechanism producing superconductivity and the potential for new applications operating at liquid nitrogen temperatures. Related driving forces are now increasing the research activity into Chevrel phase superconductors. Fundamental interest arises because these materials may offer a model (almost) cubic system in which to address non-BCS superconductivity without the strong anisotropy or layering present in the HTS materials. Furthermore Chevrel phase superconductors have interesting fundamental properties that are intermediate between the HTS and LTS materials. Technological interest arises because of the high values of B_{C2} in these materials and improvements in cryocooler technology, which facilitates operating very high-field magnets at ~ 4 K (Watanabe et al., 1998). Indeed if J_C in the wires of these materials can be improved by say a factor of ~ 8, it will open the possibility of using them in the next generation of high-field magnet systems operating in fields significantly above 25 T.

Acknowledgements

The author acknowledges helpful comments and literature from Dr. Raine as well as the research groups in Durham, Geneva and Rennes. He would also like to thank the referee who did a very welcome thorough job. Thanks also to Amanda, Emily, Peter, Alex and Michael for their support. The data are available at: http://dx.doi.org/10.15128/r1h702q636g

Further Reading

There is a very good volume of review articles dedicated to Ted Geballe for his 95th birthday – Physica C:514 1 – 444 July 2015 edited by J E Hirsch, M B Maple and F Marsiglio (Hirsch et al., 2015b). Relevant articles include:

J. E. Hirsch, M. B. Maple, and F. Marsiglio, 2015. Superconducting materials classes: Introduction and overview, *Physica C: Superconductivity* vol. 514, pp. 1–8 (Hirsch et al., 2015a). An interesting approach to classifying many of the materials that appear on the Uemura plot.

Pena O, 2015. Chevrel phases: Past, present and future, *Physica C – Superconductivity and Its Applications*, 514, 95–112. DOI: 10.1016/j.physc.2015.02.019. An excellent review of the superconductivity properties of Chevrel phase materials (Pena, 2015).

C. T. Wolowiec, B. D. White, and M. B. Maple, 2015. Conventional magnetic superconductors, *Physica C:*

Superconductivity, vol. 514, pp. 113–129 (Wolowiec et al., 2015). An interesting review of conventional magnetic superconductors that is focussed on rhodium borides, Chevrel phases and nickel-borocarbides.

K. Shimizu, 2015. Superconductivity from insulating elements under high pressure, *Physica C: Superconductivity*, vol. 514, pp. 46–49 (Shimizu, 2015). Hamlin, J J 2015. Superconductivity in the metallic elements under pressure, 514, 59–76. (Hamlin, 2015) A pair of interesting reviews that focus on elements that show a substantial increase in critical temeprature with pressure.

W. Chu, P. C. Canfield, R. C. Dynes, Z. Fisk, B. Batlogg, G. Deutscher, et al. 2015. Epilogue: Superconducting materials past, present and future, *Physica C*, vol. 514, pp. 437–443 (Chu et al., 2015). Some interesting discussions about future materials.

King R B, 1999. Chemical structure and superconductivity, *Journal of Chemical Information and Computer Science*, vol. 39, pp. 180–191 (King, 1999). An excellent review of structure and superconductivity in Chevrel phase materials and lanthanide rhodium borides.

Also:

Perrin A and Perrin C, 2012 The molybdenum and rhenium octahedral cluster chalcohalides in solid state chemistry: from condensed to discrete cluster units, *Comptes Rendus Chimie*, 15, 8125–836. An excellent and detailed review of the solid state chemistry of these materials (Perrin and Perrin, 2012).

King R B, 1999. Chemical structure and superconductivity. *Journal of chemical information and computer science*, 39, 180–191. An excellent review of chemical structure in superconducting materials (King, 1999).

Evetts J, 1992. Concise Encyclopaedia of Magnetic and Superconducting Materials. (Pergamon Press UK). A series of compact, introductory articles predominantly on the science and technology of magnetic and superconducting materials (Evetts, 1992).

PenaO Sergent M, 1989. Rare earth based Chevrel phases REMo6X8: Crystal growth, physical and superconducting properties, *Progress in Solid State Chemistry*, 19, 165–281. A very interesting comprehensive review of single crystal growth and properties. Great detail is provided about the chemistry and materials science of rare earth materials (Peña and Sergent, 1989).

Fischer Ø and Maple M B, 1982, Superconductivity in Ternary Compounds Vol.I – Structural, Electronic and Lattice Properties and Vol II – Superconductivity and Magnetism (Springer-Verlag Berlin Heidelberg). These two volume texts were written by many of the individual researchers involved in the intensive research of the seventies. The texts include an excellent compendium of many of the material properties for Chevrel phase superconductors – rather than extend our reference list considerably we have quoted these texts as a source rather cite the several hundred papers quoted therein (Fischer and Maple, 1982a, b).

Fischer Ø, 1978. Chevrel phases: Superconducting and normal state properties, *Applied Physics*, 16, 1–28. Excellent older review of the properties of Chevrel phase superconductors (Fischer, 1978).

References

Abrikosov AA (2000). Theory of high-T_C superconducting cuprates based on experimental evidence. Physica C 341-348:97–102.

Alekseevskii NE, Nizhankowski VL, Beille J, Lacheisserie E (1988) Investigation of the thermal expansion, electrical resistivity, and magnetic susceptibility anisotropy in $PbMo_6S_8$ single crystals. Journal of Low Temperature Physics 72:241–246.

Alterovitz SA, Woolam JA (1978) Upper critical field of copper molybdenum sulphide. Solid State Communications 25:141–144.

Anderson PW (2006) The 'strange metal' is a projected Fermi liquid with edge singularities. Nature 2:626–630.

Aruchamy A, Tamaoki H, Fujisjhima A, Berger H, Speziali NL, Levy F (1994) Photoelectrochemical characterization of a rhenium octahedral cluster compound $[Re_6Se_7Br_4]$. Materials Research Bulletin 29:359–368.

Aurbach D, Lu Z, Schechter A, Gofer Y, Turgeman R, Cohen Y, Moshkovich M, Levi E (2000) Protoype systems for rechargeable magnesium batteries. Nature 407:724–727.

Bader SD, Knapp GS, Sinha SK, Schweiss P, Renker B (1976) Phonon spectra of Chevrel-phase lead and tin molybdenum sulfides: A molecular-crystal model and its implications for superconductivity. Physical Review Letters 37:344–348.

Bardeen J, Cooper LN, Schrieffer JR (1957) Theory of Superconductivity. Physical Review 108:1175–1204.

Batlogg B, Cava RJ, Jayaraman A, van Dover RB, Kourouklis GA, Sunshine S, Murphy DW, Rupp LW, Chen HS, White A, Short KT, Mujsce AM, Rietman EA (1987) Isotope effect in the High-T_C superconductors $Ba_2YCu_3O_7$ and $Ba_2EuCu_3O_7$. Physical Review Letters 58:2333–2336.

Batterman BW, Barrett CS (1964) Crystal Structure of Superconducting V_3Si. Physical Review Letters 13:390–392.

Bean CP (1962) Magnetization of hard superconductors. Physical Review Letters 8:250–253.

Beille J, Schmitt H, Padiou J, Sergent M (1991) The superconducting state of $Sr_xMo_6S_8$ (x<1) by simultaneous application of chemical and external pressure. Journal of Physics C – Solid State 3:2471–2477.

Benson JW, Schrader GL, Angelici RJ (1995) Studies of the mechanism of thiophene hydrodesulfurization:2H NMR and mass spectral analysis of 1,3-butadiene produced in the deuterodesulfurization (DDS) of thiophene over $PbMo_6S_8$ catalyst. Journal of Molecular Catalysis A: Chemical 96:283–299.

Birrer P, Gygax FN, Hitti B, Lippelt E, Schenck A, Weber M, Cattani D, Cors J, Decroux M, Fischer Ø (1993) Magnetic penetration depth in the Chevrel-phase superconductors $SnMo_6S_{8-x}$ and $PbMo_6S_{8-x}Se_x$. Physical Review B 48:16589–16599.

Blount EI, Varma CM (1979) Electromagnetic effects near the superconductor-to-ferromagnet transition. Physical Review Letters 42:1079–1082.

Bonney LA, Willis TC, Larbalestier DC (1995) Dependence of critical current density on microstructure in the $SnMo_6S_8$ Chevrel-phase superconductor. Journal of Applied Physics 77:6377–6387.

Boursicot S, Bouquet V, Péron I, Guizouarn T, Potel M, Guilloux-Viry M (2012) Synthesis of $Cu_2Mo_6S_8$ powders and thin films from intermediate oxides prepared by polymeric precursor method. Solid State Sciences 14:719–724.

Bullett DW (1977) Relation between electronic structure and T_C in binary and ternary molybdenum chalcogenides. Physical Review Letters 39:664–666.

Caillat T, Fleurial JP, Snyder GJ (1999) Potential of Chevrel phases for thermoelectric applications. Solid State Science 1:535–544.

Capone II DW, Guertin RP, Foner S, Hinks DG, Li HC (1984) Effect of pressure and oxygen defects in divalent Chevrel-phase superconductors. Physical Review B 29:6375–6377.

Carty GJ, Hampshire DP (2008) Visualising the mechanism that determines the critical current density in polycrystalline superconductors using time-dependent Ginzburg-Landau theory. Physical Review B 77:172501.

Carty GJ, Hampshire DP (2013) The critical current density of an SNS junction in high magnetic fields. Superconductor Science and Technology 26:065007.

Cattani D, Cors J, Decroux M, Fischer Ø (1991) Intra- and intergrain critical current in $PbMo_6S_8$ sintered samples. IEEE Transactions on Magnetics 27:950–953.

Cattani D, Cors J, Decroux M, Seeber B, Fischer Ø (1988) Calorimetric determination of H_{C2} of $PbMo_6S_8$. Physica C 153:461–462.

Cave J (1998) Handbook of Applied Superconductivity, 1st Edition. Bristol: Institute of Physics.

Cheggour N, Decroux M, Fischer Ø, Hampshire DP (1998) Irreversibility line and granularity in Chevrel phase superconducting wires. Journal of Applied Physics 84:2181–2183.

Cheggour N, Deroux M, Gupta A, Fischer Ø, Pederboom JAAJ, Bouquet V, Sergent M, Chevrel R (1997) Enhancement of the critical current density in Chevrel phase superconducting wires. Journal of Applied Physics 81:6277–6284.

Cheggour N, Decroux M, Gupta A, Ritter S, Schrœter V, Seeber B, Flükiger R, Fischer Ø, Boudjada S, Burel L, Bouquest V, Chevrel R, Sergent M, Massat H, Langlois P, Genevey P (1993) Superconducting properties of $PbMo_6S_8$ wires with micron grain size obtained from the decomposition of Mo_6S_8. Proceedings of ICMAS 93:403–408.

Chen X, Perel AS, Brooks JS, Guertin RP, Hinks DG (1993) Specific heat measurements of pressure-induced reentrant superconductivity in $Eu_{0.9}Ho_{0.1}Mo_6S_8$. Journal of Applied Physics 73:1886–1891.

Cheng Y, Luo L, Zhong L, Chen JT, Li B, Wang W, Mao SX, Wang CY, Sprenkle VL, Li G, Liu J (2016) Highly reversible Zinc-ion intercalation into Chevrel phase Mo_6S_8 nanocubes and applications for advanced Zinc-ion batteries. Applied Materials and Interfaces 9:13673–13677.

Chevrel R, Sergent M (1982) Chemistry and structure of ternary molybdenum chalcogenides. In: Superconductivity in ternary compounds I: Structural, electronic and lattice properties (Fischer Ø, Maple MB, eds), pp. 25–86.

Chevrel R, Sergent M, Prigent J (1971) Sur de Nouvelles Phases Sulfurées Ternaires du Molybdène. Journal of Solid State Chemistry 3:515–519.

Chevrel R, Sergent M, Prigent J (1974) Un nouveau sulfure de molybdène: Mo_3S_4 preparation, propriétés et structure cristalline. Materials Research Bulletin 9:1487–1498.

Chu CW, Huang SZ, Lin CH, Meng RL, Wu MK, Schmidt PH (1981) High-pressure study of the anomalous rare-earth ternaries $Eu_{1.2}Mo_6S_8$ and $Eu_{1.2}Mo_6Se_8$. Physical Review Letters 46:276–279.

Chu CW, Canfield PC, Dynes RC, Fisk Z, Batlogg B, Duetscher G, Geballe TH, Zhao ZX, Greene RL, Hosono H, Maple MB (2015) Epilogue: Superconducting materials past, present and future. Physica C 514:437–443.

Cohen RW, Cody GD, Halloran JJ (1967) Effect of Fermi-level motion on normal state properties of Beta-tungsten superconductors. Physical Review Letters 19:840–844.

Corrignan A, Hamard C, Pena O (1999) Superconducting properties of Solid Solutions $(Mo_6Se_8)Pb_x$ and $Pb_xMo_6Se_8$ in the ternary system Pb-Mo-Se. Journal of Alloys and Compounds 289:260–264.

Cors J, Cattani D, Decroux M, Stettler A, Fischer Ø (1990) The critical field of $PbMo_6S_8$ measured by specific heat up to 14 T. Physica B 165:1521–1522.

Dallacasa V, Feduzi R (1992) Quantum percolation of high Tc materials: Tc dependence on carrier density. Physics Letters A 170:153–158.

Daniel IJ, Hampshire DP (2000) Harmonic calculations and measurements of the irreversibility field using a vibrating sample magnetometer. Physical Review B 61:6982–6993.

Daniel IJ, Zheng DN, Hampshire DP (1997) An investigation of the peak effect in the Chevrel phase superconductor tin molybdenum sulphide. IOP Appl Super Conf 2:1169–1172.

Decroux M, Fischer Ø (1982) Critical fields of ternary molybdenum chalcogenides. In: Superconductivity in Ternary Compounds II (Maple MB, Fischer Ø, eds), pp. 57–98: Springer-Verlag.

Decroux M, Fischer Ø, Flükiger R, Seeber S, Delesclefs R, Sergent M (1978) Anisotropy of H_{C2} in the Chevrel phases. Solid State Communications 25:393–396.

Decroux M, Selvam P, Cors J, Seeber B, Fischer Ø, Chevrel R, Rabiller P, Sergent M (1993) Overview on the recent progress of Chevrel phases and their impact on the development of $PbMo_6S_8$ wires. IEEE Transactions on Applied Superconductivity 3:1502–1509.

Decroux M, Antognazza L, Kugler M, Koller E, Fischer Ø, Lemee N, Guilloux-Viry M, Perrin A (1999) Investigation of vortex dynamics close to B_{C2} in $Cu_2Mo_6S_8$ quasi epitaxial thin films. Solid State Sciences 1:585–589.

Dew-Hughes D (1974) Flux pinning mechanisms in type II superconductors. Philosophical Magazine 30:293–305.

DeWilde Y, Miyakawa N, Guptasarma P, Iavarone M, Ozyuzer L, Zasadzinski JF, Romano P, Hinks DG, Kendziora C, Crabtree GW, Gray KE (1998) Unusual strong-coupling effects in the tunneling spectroscopy of optimally doped and overdoped $Bi_2Sr_2CaCu_2O_8$. Physical Review Letters 80:153–156.

Ding H, Yokoya T, Campuzano JC, Takahashi T, Randeria M, Norman MR, Mochiku T, Kadowaki K, Giapintzakis J (1996) Spectroscopic evidence for a pseudogap in the normal state of underdoped high-Tc superconductors. Nature 382:51–54.

Dubois C, Petrovic AP, Santi G, Berthod C, Manuel AA, Decroux M, Fischer Ø, Potel M, Chevrel R (2007) Node-like excitations in superconducting $PbMo_6S_8$ probed by scanning tunneling spectroscopy. Physical Review B 75:104501.

Dzhumanov S, Karimboev EX, Djumanov SS (2016) Underlying mechanisms of pseudogap phenomena and Bose-liquid superconductivity in high-Tc cuprates. Physics Letters A 380:2173–2180.

Eastell C (1998) Microstructure and properties of high temperature superconducting wires. In: Materials Department: Thesis: Oxford University.

Eisaki H, Takagi H, Cava RJ, Batlogg B, Krajewski JJ, Peck WF, Mizuhashi K, Lee JO, Uchida S (1994) Competition between magnetism and superconductivity in rare-earth nickel boron carbides. Physical Review B 50:647–650.

Even-Boudjada S, Burel L, Chevrel R, Sergent M (1998a) New synthesis route of $PbMo_6S_8$ superconducting Chevrel phase from ultrafine precursor mixtures: II PbS, Mo_6S_8 and Mo powders. Materials Research Bulletin 33:419–431.

Even-Boudjada S, Burel L, Chevrel R, Sergent M (1998b) New synthesis route of $PbMo_6S_8$ superconducting Chevrel phase from ultrafine precursor mixtures: I. PbS, MoS_2 and Mo powders. Materials Research Bulletin 33:237–252.

Even-Boudjada S, Tranchant V, Chevrel R, Sergent M, Crosnier-Lopez M, Laligant Y, Retoux R, Decroux M (1999) One of the possible explanations of the major J_c limiting factor at the $PbMo_6S_8$ granular superconductor grains surface. Materials Letters 38:90–97.

Evetts J (1992) Concise Encyclopedia of Magnetic and Superconducting Materials: Pergamon.

Fietz WA, Webb WW (1967) Magnetic properties of some Type-II alloy superconductors near the upper critical field. Physical Review 161:423–433.

Fischer Ø (1978) Chevrel phases – superconducting and normal state properties. Applied Physics 16:1–28.

Fischer Ø, Maple MB (1982a) Superconductivity in Ternary Compounds Vol I - Structural, Electronic and Lattice Properties, 1st Edition. Berlin: Springer-Verlag.

Fischer Ø, Maple MB (1982b) Superconductivity in Ternary Compounds Vol II - Superconductivity and Magnetism. Berlin: Springer Verlag.

Fischer Ø, Treyvaud A, Chevrel R, Sergent M (1975a) Superconductivity in the $RE_xMo_6S_8$. Solid State Communications 17:721–724.

Fischer Ø, Decroux M, Roth S, Chevrel R, Sergent M (1975b) Compensation of the paramagnetic effect on H_{C2} by magnetic moments: 700 kG superconductors. Journal of Physics C – Solid State 8:L474–L477.

Fisk Z, Webb GW (1976) Saturation of the high temperature normal state electrical resistivity of superconductors. Physical Review Letters 36:1084–1086.

Fleurial JP, Snyder G, Borshchevsky A, Caillat T (2002) Thermoelectric materials formed based on Chevrel phases. In: Google Patents.

Flükiger R, Baillif R (1982) Metallurgy and Structural transformations in ternary molybdenum chalcogenides. In: Superconductivity in Ternary Compounds Vol I - Structural, Electronic and Lattice Properties (Fischer Ø, Maple MB, eds), pp. 113–141.

Flükiger R (2010) Procedure of densifying filaments for a superconductive wire. In: Google Patents.

Foner S, McNiff EJ, Jr, Alexander EJ (1974) 600kG superconductors. Physics Letters 49A:269–270.

Fradin FY, Knapp GS, Bader SD, Cinader G, Kimball CW (1976) Electron and Phonon Properties of A-15 Compounds and Chevrel Phases. In: D.H. Douglass (Ed.), Superconductivity in d- and f-Band Metals: Second Rochester Conference, Springer US, Boston, MA: 297–312.

François M, Yvon K, Cattani D, Decroux M, Chevrel R, Sergent M, Boudjada S, Wroblewski T (1994) Synchrotron powder diffraction study of the low-temperature lattice distortion of $PbMo_6S_8$. Journal of Applied Physics 75:423–430.

Fumagalli P, Schoenes J (1991) Magneto-optical Kerr-effect study of the high-field superconductors $Eu_{1-x}Pb_xMo_6S_8$ and $Eu_{1-x}Sn_xMo_6S_{8-y}Se_y$. Physical Review B 44:2246–2262.

Furuyama M, Kobayashi N, Muto Y (1989) Electron-phonon interactions in the superconducting Chevrel phase compounds $Mo_6Se_{8-x}S_x$. Physical Review B 40:4344–4354.

Geantet C, Horyn R, Padiou J, Pena O, Sergent M (1990) Single crystal studies of $REMo_6S_8$ (RE = Er, Lu). Physica B 163:431–434.

Geng L, Lv G, Xing X, Guo J (2015) Reversible electrochemical intercalation of aluminum in Mo6S8. Chemistry of Materials 27:4926–4929.

Ginzburg VL (1957) Ferromagnetic superconductors. Soviet Physics JETP 4:153–160.

Goldacker W, Specking W, Weiss F, Rimikis G, Flükiger R (1989b) Influence of transverse, compressive and axial tensile stress on the superconductivity of $PbMo_6S_8$ and $SnMo_6S_8$ wires. Cryogenics 29:955–960.

Goldacker W, Specking W, Weiss F, Rimikis G, Flükiger R (1990) Effect of Axial Tensile and Transverse Compressive Stress on J_c and B_{c2} of $PbMo_6S_8$ and $SnMo_6S_8$ wires. In: Reed R.P., Fickett F.R. (eds) Advances in Cryogenic Engineering Materials. An International Cryogenic Materials Conference Publication, vol 36. Springer, Boston, MA. https://doi.org/10.1007/978-1-4613-9880-6_46

Goncalves AP, Godart C (2014) New promising bulk thermoelectrics: Intermetallics, pnictides and chalcogenides. European Physics Journal B 87:42.

Gorter CJ, Casimir HBG (1934) 2 fluid model. Physikalische Zeitschrift 35:963–966.

Gougeon P, Pena O, Potel M, Sergent M, Brusetti R (1984) New ternary $M_{(2n-2)}Mo_{6n}X_{(6n+2)}$ chalcogenides (M= Rb, Cs; X= S, Se) with condensed Mo_{6n} clusters (n= 2, 3, 4, 5). Annales de chimie et de physique(Paris) 9:1079–1082.

Grant PM (1995) Superconducting superwires. Nature 375:107–108.

Gupta A, Decroux M, Selvam P, Cattani D, Willis TC, Fischer Ø (1994) Critical currents and pinning in powder metallurgically processed Chevrel phase bulk superconducting samples. Physica C 234:219–228.

Gurvitch M, Fiory AT (1987) Resistivity of $La_{1.825}Sr_{0.175}CuO_4$ and $YBa_2Cu_3O_7$ to 1100K: absence of saturation and its implications. Physics Review Letters 59:1337–1340.

Hamard C, Lancin M, Marhic C, Pena O (2002) Intergrowth between binary and ternary phases in Chevrel-phase compounds $REMo_6Se_8$ containing heavy rare-earth elements. Materials Science and Engineering: A A333:250–261.

Hamlin JJ (2015) Superconductivity in the metallic elements under pressure. Physica C: Superconductivity 514:59–76.

Hampshire D, Niu H (2005) High-field superconductors. In: Google Patents.

Hampshire DP (1998) A barrier to increasing the critical current density of bulk untextured polycrystalline superconductors in high magnetic fields. Physica C: Superconductivity and Its Applications 296:153–166.

Hampshire DP (2001) The non-hexagonal flux-line lattice in superconductors. Journal of Physics: Condensed Matter 13:6095–6113.

Hampshire DP (2020) Parameterisation of critical temperature versus carrier concentration in superconductors. In progress.

Hampshire DP, Jones H (1987) A detailed investigation of the E-J characteristic and the role of defect motion within the flux-line lattice for high-current-density, high field superconducting compounds with particular reference to data on Nb_3Sn throughout its entire field-temperature phase space. Journal of Physics C – Solid State 20:3533–3552.

Hampshire DP, Jones H, Mitchell EWJ (1985) An in-depth characterisation of $(NbTa)_3Sn$ filamentary superconductor. IEEE Transactions on Magnetics 21:289–292.

Harrison DW, Lim KC, Thompson JD, Huang CY, Hambouger PD, Luo HL (1981) Observation of the transition from semiconductor to high-T_C superconductor in $(Sn_xEu_{1-x})_y Mo_6S_8$ under high pressure. Physical Review Letters 46:280–283.

Harshman DR, Mills Jr AP (1992) Concerning the nature of high-Tc superconductivity: Survey of experimental properties and implications for interlayer coupling. Physical Review B 45:10684–10712.

Herrmann PF, Schellenberg L, Zuccone J, Seeber B, Fischer Ø, Grill R, Perenboom JAAJ (1992) Investigation of voltage steps of U(I) curves in $PbMo_6S_8$ wires. Physica C 202:61–68.

Hillier AD, Cywinski R (1997) The classification of superconductors using muon spin rotation. Applied Magnetic Resonance 13:95–109.

Hinks DG, Jorgensen JD, Li HC (1983) Structure of the oxygen point defects in $SnMo_6S_8$ and $PbMo_6S_8$. Physical Review Letters 51:1911–1914.

Hinks DG, Jorgensen JD, Li HC (1984) Oxygen impurity in the Chevrel-phase $SnMo_6S_8$. Solid State Communications 49:51–54.

Hirsch JE, Maple MB, Marsiglio F (2015a) Superconducting materials classes: Introduction and overview. Physica C: Superconductivity 514:1–8.

Hirsch JE, Maple MB, Marsiglio F (2015b) Superconducting materials: Conventional, unconventional and undetermined. Physica C: Superconductivity 514:1–444.

Holmgren DJ, Demers RT, Klein MV, Ginsberg DM (1987) Raman study of phonons in Chevrel-phase crystals. Physical Review B 36:1952–1955.

Holtzberg F, LaPlaca SJ, McGuire TR, Webb RA (1984) Magnetic susceptibility and superconductivity of single-crystal Ho-Mo-S Chevrel phase. Journal of Applied Physics 55:2013–2015.

Horyn R, Pena O, Geantet C, Sergent M (1989) Kinetics of destruction of Mo-S binary phases and crystal growth of rare-earth molybdenum chalcogenides. Superconductor Science and Technology 2:71–90.

Horyn R, Pena O, Wojakowski A, Sergent M (1994) The growth of single crystals of some $REMo_6Se_8$ superconductors. Superconductor Science and Technology 7:146–153.

Horyn R, le Berre F, Wojakowski A, Pena O (1996) Phase equilibria in the La-Mo-Se system at 1200°C in the vicinity of $LaMo_6Se_6$ and Mo_3Se_4. Superconductor Science and Technology 9:1081–1086.

Ingle NJC, Willis TC, Larbalestier DC, Meingast C (1998) Effects of hot isostatic pressing on the lattice parameters and the transition temperature of $Pb_{0.8}Sn_{0.2}Mo_6S_8$. Physica C 308:191–197.

Ishikawa M, Fischer Ø, Muller J (1982) Superconductivity and magnetism in (RE)Mo_6S_8 type compounds. In: Superconductivity in Ternary Compounds II (Maple MB, Fischer Ø, eds), pp. 143–165: Springer-Verlag.

Jaccarino V, Peter M (1962) Ultra-high-field superconductivity. Physical Review Letters 9:290–292.

Johnston DC, Shelton RN (1977) Magnetic properties of $RE_xMo_6Se_8$ compounds between 0.7 and 295 K. Journal of Low Temperature Physics 26:561–572.

Jorgensen J, Hinks DG (1985) Low temperature structural distortions in the high Tc Chevrel-phase superconductors $PbMo_6S_8$ and $SnMo_6S_8$. Solid State Communications 53:289–292.

Jorgensen JD, Hinks DG (1986) Rhombohedral-to-Triclinic phase transition in $BaMo_6S_8$. Physica B 136:485–488.

Jorgensen JD, Hinks DG, Felcher GP (1987) Lattice instability and superconductivity in the Pb, Sn and Ba Chevrel phases. Physical Review B 35:5365–5368.

Kaiser AB (1997) Comparison of thermopower behaviour in different superconductors. Physica C 282-287:1251–1252.

Kajiyana K, Matsushita T, Yamafuji K, Hamasaki K, Komata T (1985) International Symposium on Flux Pinning and Electromagnetic Properties in Superconductors. Fukuoka: Matsukuma Press Co.

Kamiguchi S, Takeda K, Kajio R, Okumura K, Nagashima S, Chihara T (2013) Application of solid-state molybdenum sulfide clusters with an octahedral metal framework to catalysis: Ring-opening of Tetrahydrofuran to Butyraldehyde. Journal of Cluster Science 24:559–574.

Kamiguchi S, Seki Y, Satake A, Okumura K, Nagashima S, Chihara T (2015) Catalytic cracking of Methyl tert-Butyl Ether to Isobutene over Bronsted and Lewis acid sites on solid-state Molydenum and Sulfide clusters with an octahedral metal framework. Journal of Cluster Science 26:653–660.

Kamihara Y, Watanabe T, Hirano M, Hosono H (2008) Iron-based layered superconductor $LaO_{1-x}F_x$ FeAs (x=0.05-0.12) with T_c=26 K. Journal of the American Chemical Society 130:3296.

Kang ZC, Eyring L, Hinode H, Uchida T, Wakihara M (1994) Structures, structural defects and reactions in a Nickel Chevrel-phase sulphide: A high resolution electron microscopy study. Journal of Solid State Chemistry 111:58–74.

Karasik V, Rikel MO, Togonidze TG, Tsebro VI (1985) Investigation of current-carrying capacity of bulk single-phase $PbMo_6S_8$ samples with grains of 0.1 micron size. Soviet Physics Solid State 27:1889–1890.

Keys SA, Hampshire DP (2003) A scaling law for the critical current density of weakly and strongly-coupled superconductors, used to parameterise data from a technological Nb_3Sn strand. Superconductor Science and Technology 16:1097–1108.

Keys SA, Cheggour N, Hampshire DP (1999) The effect of hot isostatic pressing on the strain tolerance of the critical current density found in modified jelly roll Nb_3Sn wires. IEEE Transactions on Applied Superconductivity 9:1447–1450.

Khlybov EP, Kuzmicheva GM, Evdokimova VV (1986) The structure of Mo_2S_3 and of high-pressure modifications of ternary molybdenum sulphides. Russian Journal of Inorganic Chemistry 31:627–630.

Kiefl RF, Hossain MD, Wojek BM, Dunsiger SR, Morris GD, Prokscha T, Salman Z, Baglo J, Bonn DA, Liang R, Hardy WN, Suter A, Morenzoni E (2010) Direct measurement of the London penetration depth in $YBa_2Cu_3O_{6.92}$ using low-energy mu SR. Physical Review B 81:4.

King RB (1999) Chemical structure and superconductivity. Journal of Chemical Information and Computer Science 39:180–191.

Kleiner WH, Roth LM, Autler SH (1964) Bulk solution of Ginzburg-Landau equations for Type II superconductors: Upper critical field region. Physical Review 133:A1226–A1227.

Kondo T, Khasanov R, Takeuchi T, Schmalian J, Kaminski A (2009) Competition between the pseudogap and superconductivity in the High-T_C copper oxides. Nature Letters 457:296–300.

Koo KF, Schewe-Miller IM, Schrader GL (1995) Reactive sputter deposition of lead Chevrel phase thin films. In: Google Patents.

Krabbes G, Oppermann H (1981) The phase diagram of the Pb-Mo-S system at 1250 K and some properties of the superconducting $PbMo_6S_8$. Crystal Research and Technology 16:777–784.

Kramer EJ (1973) Scaling laws for flux pinning in hard superconductors. Journal of Applied Physics 44:1360–1370.

Kramer EJ (1975) Microstructure - critical current relationships in hard superconductors. Journal of Electronic Materials 4:839–879.

Kubo Y, Uchikawa F, Utsunomiya S, Noto K, Katagiri K, Kobayashi N (1993) Fabrication and evaluation of small coils using $PbMo_6S_8$ wires. Cryogenics 33:883–888.

Kumta PN, Saha P, Datta MK, Manivannan A (2015) Cathodes and electrolytes for rechargeable magnesium batteries and methods of manufacture. In: Google Patents.

Lachal A, Junod A, Muller J (1984) Heat capacity analysis of a large number of Chevrel-type superconductors. Journal of Low Temperature Physics 55:195–232.

Lachal B, Bailif R, Junod A, Muller J (1983) Structural instabilities of Chevrel phases: the alkaline earth molybdenum sulphide series. Solid State Communications 45:849–851.

Le Berre F, Hamard C, Pena O, Wojakowski A (2000) Structural studies on single crystals of Chevrel phase selenides $REMo_6Se_8$ (RE: La, Ce, Pr, Nd, or Sm) at 298 K. Inorganic Chemistry 39:1100–1105.

Le Berre F, Maho F, Pena O, Horyn R, Wojakowski A (1995) Physical and structural properties of Chevrel-phase selenides Mo_3Se_4 and $RE_xMo_6Se_8$: Crystal growth and mutual solubility. Journal of Magnetism and Magnetic Materials 140-144 1171–1172.

Le Berre F, Pena O, Hamard C, Corrignan A, Horyn R, Wojakowski A (1997) New superconducting materials based upon doping of the Chevrel phase binary compound Mo_6Se_8. Journal of Alloys and Compounds 262:331–334.

Le Berre F, Pena O, Perrin C, Padiou J, Horyn R, Wojakowski A (1998a) Novel crystal structure in the Chevrel-phase compound $EuMo_6Se_8$. Transport and magnetic properties. Journal of Alloys and Compounds 280:85–93.

Le Berre F, Pena O, Perrin C, Sergent M, Horyn R, Wojakowski A (1998b) Single-crystal studies of the Chevrel-phase superconductor $La_xMo_6Se_8$ - I: Correlation between T_C and the interatomic distances. Journal of Solid State Chemistry 136:151–159.

Le Berre F, Tshimanga D, Giulloux AL, Leclercq J, Sergent M, Pena O, Hiryn R, Wojakowski A (1996) Rare-earth doping of the Mo_3Se_4 superconductor. Physica B 228:261–271.

Le Lay L, Willis TC, Larbalestier DC (1991) Magnetization properties of a $SnMo_6S_8$ single crystal. IEEE Transactions on Magnetics 27:954–957.

Leigh NR (2001) Specific heat measurements on Chevrel phase materials exhibiting coexistence of superconductivity and magnetism. In: Department of Physics, p. 143. Durham: University of Durham.

Lemee N, Guilloux-Viry M, Perrin A, Sergent M (1998) Superconducting $Cu_2Mo_6S_8$ thin films deposited in-situ by laser ablation on R-plane sapphire. The European Physical Journal Applied Physics 1:197–201.

Levi E, Gofer Y, Aurbach D (2010) On the way to rechargeable Mg batteries: The challenge of new cathode materials. Chemistry of Materials 22:860–868.

Loram JW, Luo J, Cooper JR, Liang WY, Tallon JL (2001) Evidence on the pseudogap and condensate from the electronic specfic heat. Journal of Physics and Chemistry of Solids 62:59–64.

Luhman T, Dew-Hughes D (1978) Superconducting wires of $PbMo_{5.1}S_6$ by a powder technique. Journal of Applied Physics 49:936–938.

Majkrzak CF, Shirane G, Thomlinson W, Ishikawa M, Fischer Ø, Moncton DE (1979) A neutron diffraction study of the coexistence of antiferromagnetism and superconductivity in $GdMo_6S_8$. Solid State Communications 31:773–775.

Mancour-Billah A, Chevrel R (2003) A new increasing delocalization of M=3d-elements (TI, Fe, Co) in the channels network of the ternary $M_yMo_6Se_8$ Chevrel phases. Journal of Solid State Chemistry 170:281–288.

Mattheis LF (1973) Band structures of transition-metal-dichalcogenide layer compounds. Physical Review B 8:3719–3740.

Mattheis LF, Fong CY (1977) Cluster model for the electronic structure of the Chevrel-phase comnpound $PbMo_6S_8$. Physical Review B 15:1760–1768.

Matthias BT, Marezio M, Corenwitt E, Cooper AS, Barz HE (1972) High-temperature superconductors, the first ternary system. Science 175:1465–1466.

Meul HW (1986) On the unusual physical properties of europium-based molybdenum chalcogenides and related Chevrel compounds. Helvetica Physica Acta 59:417–489.

Miraglia S, Goldacker W, Flükiger R, Seeber B, Fischer Ø (1987) Thermal expansion studies in the range 10 K - 1200 K in $PbMo_6S_8$ by means of X-ray diffraction. Materials Research Bulletin 22:795–802.

Mitelman A, Levi MD, Lancry E, Levi E, Aurbach D (2007) New cathode materials for rechargeable Mg batteries; fast Mg ion transport asnd reversible extrusion in $Cu_yMo_6S_8$ compounds. Chemical Communications 41:4212–4214.

Morales F, Escudero R, Briggs A, Monceau P, Horyn R, Le Berre F, Pena O (1996) Point contact spectroscopy on the ferromagnetic superconductor $HoMo_6S_8$. Physica B 218:193–196.

Morley NA, Leigh NR, Niu H, Hampshire DP (2001) High upper critical field in the Chevrel phase superconductor lead-molybdenum-sulphide doped with europium. IEEE Transactions on Applied Superconductivity 11:3599–3602.

Murgia F, Antitomaso P, Stievano L, Monconduit L, Berthelot R (2016) Express and low-cost microwave synthesis of the ternary Chevrel phase $Cu_2Mo_6S_8$ for application in rechargeable magnesium batteries. Journal of Solid State Chemistry 242:151–154.

Nakamura T, Hanayama Y, Kiss T, Vysotsky V, Okamoto H, Matsushita T, Takeo M, Irie F, Yamafuji K (1997) Current-voltage characteristics in YBaCuO thin films over more than 13 decades of electric-field. Institute of Physics Conference Series No 158:1017–1020.

Nespolo M, Aroyo MI, Souvignier B (2018) Crystallographic shelves: space-group hierarchy explained. Journal of Applied Crystallography 51:1481–1491.

Niu H, Leigh N, Hampshire D (2002) Superconducting properties of quaternary Chevrel phase $Pb_{1-x}Cu_{1.8x}Mo_6S_8$ - Private Communication.

Niu HJ, Morley NA, Hampshire DP (2001) Chevrel phase $(Pb_{1-x}Cu_{1.8x})Mo_8S_6$ with a mixed structure and high critical parameters. IEEE Transactions on Applied Superconductivity 11:3619–3622.

Nunes RW, Mazin II, Singh DJ (1999) Theoretical search for Chevrel-phase-based thermoelectric materials. Physical Review B 59:7969–7972.

Ohta M, Yamamoto A, Obara H (2009a) Thermoelectrfic properties of Chevrel-phase sulfides $M_xMo_6S_8$ (M: Cr, Mn, Fe, Ni). Journal of Electronic Materials 39:2117–2121.

Ohta M, Obara H, Tamamoto A (2009b) Preparation and thermoelectric properties of Chevrel-phase $CuxMo_6S_8$ ($2.0 < x < 4.0$). Materials Transactions 50:2129–2123.

Ohtaki R, Zhao BR, Luo HR (1984) Superconducting tunneling on $Cu_xMo_6S_8$ films. Journal of Low Temperature Physics 54:119–127.

Pazol BG, Holmgren DJ, Ginsberg DM (1989) Upper critical field anisotropy in the Chevrel phase compound $PbMo_6S_8$. Journal of Low Temperature Physics 74:133–140.

Pellizone M, Treyvaud A, Spitzli P, Fischer Ø (1977) Magnetic susceptibility of $(Rare\ Earth)_xMo_6S_8$. Journal of Low Temperature Physics 29:453–465.

Pena O (2015) Chevrel phases: Past, present and future. Physics C 514:95–112.

Pena O, Mancour-Billah A, Chevrel R (2009) Single crystal studies of ternary transition-metal molybdenum selenides MMo_6S_8 (M=Ti, Fe, Mn, Cr and Co). Journal of Cluster Science 20:51–62.

Pena O, Geantet C, Schmitt H, Le Berre F, Hamard C (1999) Structural properties of rare-earth molybdenum chalcogenides $REMo_6X_8$. Solid State Sciences 1:577–584.

Peña O, Sergent M (1989) Rare earth based Chevrel phases $REMo_6X_8$: Crystal growth, physical and superconducting properties. Progress in Solid State Chemistry 19:165–281.

Peña O, Le Berre F, Padiou J, Marchand T, Horyn R, Wojakowski A (1998) Single-crystal studies of the Chevrel-phase superconductor $La_xMo_6Se_8$ - II: Physical and superconducting properties. Journal of Solid State Chemistry 136:160–166.

Perrin A, Perrin C (2012) The molybdenum and rhenium octahedral cluster chalcogenides in solid state chemistry: From condensed to discrete cluster units. Comptes Rendus Chimie 15:815–836.

Perrin C, Chevrel R, Sergent M (1979) Etude structurale d'un thiohalogenure supraconducteur derivant du Mo II: $Mo_6S_6Br_2$. Materials Research Bulletin 14:1505–1515.

Petrovic AP, Lortz R, Santi G, Berthod C, Dubois C, Decroux M, Demuer A, Antunes AB, Pare A, Salloum D, Gougeon P, Potel M, Fischer O (2011) Multiband superconductivity in the Chevrel phases $SnMo_6S_8$ and $PbMo_6S_8$. Physics Review Letters 106:017003.

Pobell F, Rainer D, Wuhl H (1982) Electron-phonon interaction in Chevrel phase compounds. In: Topics in Current Physics - Superconductivity in Ternary Compounds Vol I (Fischer Ø, Maple MB, eds), pp. 251–277. Berlin: Springer-Verlag.

Poppe U, Wuhl H (1981) Tunneling spectrocopy on the superconducting Chevrel-phase compounds $Cu_{1.8}Mo_6S_8$ and $PbMo_6S_8$. Journal of Low Temperature Physics 43:371 370–382.

Prober DE, Schwall RE, Beasley MR (1980) Upper critical fields and reduced dimensionality of the superconducting layered compounds. Physical Review B 21:2717–2733.

Ramsbottom HD, Hampshire DP (1997) Improved critical current density and irreversibility line in HIP'ed Chevrel phase superconductor $PbMo_6S_8$. Physica C 274:295–303.

Ramsbottom HD, Hampshire DP (1999) Flux Penetration measurements and the harmonic magnetic response of hot isostatically pressed $(Pb,Gd)Mo_6S_8$. Journal of Applied Physics 85:3732–3739.

Renner C, Revaz B, Genoud JY, Kadowaki K, Fischer Ø (1998) Pseudogap Precursor of the Superconducting Gap in Under- and Overdoped $Bi_2Sr_2CaCu_2O_{8+d}$. Physical Review Letters 80:149–152.

Rimikis G, Goldacker W, Specking W, Flükiger R (1991) Critical currents in $Pb_{1.2-x}Sn_xMo_6S_8$ wires. IEEE Transactions on Magnetics 27:1116–1119.

Roche C, Chevrel R, Jenny A, Pecheur P, Scherrer H, Scherrer S (1999) Crystallography and density of states calculation of MxMo6Se8 (M=Ti, Cr, Fe, Ni). Physical Review B 60:16442–16447.

Rossel C, Fischer Ø (1984) Critical current densities in bulk Chevrel-phase samples. Journal of Physics F: Metal Physics 14:455–472.

Rossel C, Pena O, Schmitt H, Sergent M (1991) On the irreversibility line in the Chevrel phase superconductors. Physica C 181:363–368.

Rybicki D, Jurkutat M, Reichardt S, Kapusta C, Haase J (2016) Perspective on the phase diagram of cuprate high-temperature superconductors. Nature Communications:1–6.

Schauer W, Schelb W (1981) Improvement of Nb_3Sn high field critical current by a two-stage reaction. IEEE Transactions on Magnetics 17:374–377.

Scurty F, Ishmael S, Flanagan G, Schwartz J (2016) Quench detection for high temperature superconductor magnets: a novel technique based on Rayleigh-backscattering interrogated optical fibres. Superconductor Science and Technology 29:03LT01.

Seeber B (2015) Ternary molybdenum chalcogenide superconducting wire and manufacturing thereof. In: Google Patents.

Seeber B, Erbuke L, Schroeter V, Perenboom JAAJ, Grill R (1995) Critical current limiting factors of hot isostatically pressed (HIP'ed) $PbMo_6S_8$ wires. IEEE Transactions on Applied Superconductivity 5:1205–1208.

Selvam P, Cors J, Cattani D, Decroux M, Fischer Ø, Seibt EW (1995) Homogeneity and critical current density of Sn-doped $PbMo_6S_8$ superconductors. Applied Physics A 61:615–621.

Selvam P, Cattani D, Cors J, M D, Niedermann P, Fischer Ø, Chevrel R, Pech T (1993) The role of Sn addition on the improvement of Jc in $PbMo_6S_8$. IEEE Transactions on Applied Superconductivity 3:1575–1578.

Selvam P, Cattani D, Cors J, Decroux M, Junod A, Niedermann P, Ritter S, Fischer Ø, Rabiller P, Chevrel R (1992) Superconducting, microstructural and grain boundary properties of hot-pressed $PbMo_6S_8$. Journal of Applied Physics 72:4232–4239.

Sergent M, Chevrel R, Rossel C, Fischer Ø (1978) On the superconductivity of $PbMo6S_8$ and the series $M_xPbMo_6S_8$ and $M_xPb_{1-x}Mo_6S_8$. Journal of the Less Common Metals 58:179–193.

Sergent M, Chevrel R, Padiou J, Pena O, Barathe R, Hirrien M, Massat H, Pech T, Turck B, Dubots P, Couach M (1984) Preparation and predevelopment of superconductors so called Chevrel phases. Annales de Chimie Science des Matériaux 9:1069–1074.

Shelton RN (1976) The effect of high pressure on superconducting ternary molybdenum chalcogenides. In: 2nd Rochester Conference on Superconductivity in d- and f-Band Metals (Douglas DH, ed), pp 137–160. New York: Plenum Press.

Shelton RN, McCallum RW, Adrian H (1976) Superconductivity in rare earth molybdenum selenides. Physics Letters 56A:213–214.

Shimizu K (2015) Superconductivity from insulating elements under high pressure. Physica C: Superconductivity 514:46–49.

Smeu M, Hossain MS, Wang ZZ, Timoshevskii V, Bevan KH, Zaghib K (2016) Theoretical investigation of Chevrel phase materials for cathodes accommodating Ca^{2+} ions. Journal of Power Sources 306:431–436.

Sonier JE, Brewer JH, Kiefl RF (2000) Mu SR studies of the vortex state in type-II superconductors. Review of Modern Physics 769–811.

Sunandana CS (1979) On the electrical resistivity of Chevrel phases. Journal of Physics C 12:L165–L168.

Sunwong P, Higgins JS, Tsui Y, Raine MJ, Hampshire DP (2013) The critical current density of grain boundary channels in polycrystalline HTS and LTS superconductors in magnetic fields. Superconductor Science and Technology 26:095006.

Tallon JL, Loram JW (2001) The doping dependence of T* - what is the real high-T-c phase diagram? Physica C – Superconductivity and Its Applications 349:53–68.

Taylor DMJ, Hampshire DP (2005) The scaling law for the strain dependence of the critical current density in Nb_3Sn superconducting wires. Superconductor Science and Technology 18:S241–S252.

Thomlinson W, Shirane G, Moncton DE, Ishikawa M, Fischer Ø (1981) Magnetic order in superconducting $TbMo_6S_8$, $DyMo_6S_8$ and $ErMo_6S_8$. Physical Review B 23:4455–4462.

Uchida T, Wakihara M (1991) Thermal behaviour of the Chevrel phase sulphides. Thermochimica Acta 174:201–221.

Uemura YJ (2004) Condensation, excitation, pairing, and superfluid density in high-T-c superconductors: The magnetic resonance mode as a roton analogue and a possible spin-mediated pairing. Journal of Physics: Condensed Matter 16:S4515–S4540.

Uemura YJ (2009) Commonalities in phase and mode. Nature Materials 8:253–255.

Uemura YJ, Le LP, Luke GM, Sternlieb BJ, Wu WD, Brewer JH, Riseman TM, Seaman CL, Maple MB, Ishikawa M, Hinks DG, Jorgensen JD, Saito G, Yamochi H (1991) Basic similarities among cuprate, bismuthate, organic, Chevrel-phase, and heavy-fermion superconductors shown by penetration-depth measurements. Physical Review Letters 66:2665–2668.

van der Meulen HP, Perenboom JAAJ, Berendschot TTJM, Cors J, Decroux M, Fischer Ø (1995) Specific heat of $PbMo_6S_8$ in high magnetic field. Physica B 211:269–271.

Wang G, Raine MJ, Hampshire DP (2017) How resistive must grain-boundaries be to limit J_C in polycrystalline superconductors? Superconductor Science and Technology 30:104001.

Watanabe K, Awaji S, Motokawa M, Mikami Y, Sakuraba J, Watzawa K (1998) 15 T cryocooled Nb_3Sn superconducting magnet with a 52 mm room temperature bore. Japanese Journal of Applied Physics 37:L1148–L1150.

Webb AW, Shelton RN (1978) Compressibilities and volume dependence of Tc for eleven Chevrel phase superconductors. Journal of Physics F: Metal Physics 8:261–269.

Werthamer NR, Helfand E, Hohenberg PC (1966) Temperature and purity dependence of the superconducting critical field, H_{c2}. III. Electron spin and spin-orbit effects. Physical Review 147:295–302.

Williams GVM, Tallon JL, Haines EM, Michalak R, Dupree R (1997) NMR evidence for a d-wave normal-state pseudogap. Physical Review Letters 78:721–724.

Willis TC, Jablonski PD, Larbalestier DC (1995) Hot isostatic pressing of Chevrel phase bulk and hydrostatically extruded wire samples. IEEE Transactions on Applied Superconductivity 5:1209–1213.

Wolf B, Molter J, Bruls G, Luthi B, Jansen L (1996) Elastic properties of superconducting Chevrel-phase compounds. Physical Review B 54:348–352.

Wolowiec CT, White BD, Maple MB (2015) Conventional magnetic superconductors. Physica C: Superconductivity 514:113–129.

Woollam JA, Somoano RB (1976) Superconducting critical fields of alkali and alkaline-earth intercalates of MoS_2. Physical Review B 13:3843–3853.

Yamamoto S, Wakihara M, Taniguchi M (1985) Phase relations in the Pb-Mo-S ternary system at 1000°C and the superconductivity of $PbMo_6S_{8-y}$. Materials Research Bulletin 20:1493–1500.

Yamasaki H, Kimura Y (1986) The phase field of the Chevrel phase $PbMo_6S_8$ at 900°C and some superconducting and structural properties. Materials Research Bulletin 21:125–135.

Yamasaki H, Umeda M, Kosaka S (1992) High critical current densities reproducibly observed for hot-isostatic-pressed $PbMo_6S_8$ wires with Mo barriers. Journal of Applied Physics 72:1–3.

Yamasaki H, Umeda M, Kosaka S, Kimura Y, Willis TC, Larabalestier DC (1991) Poor intergrain connectivity of $PbMo_6S_8$ in sintered Mo-sheathed wires and the beneficial effect of hot-isostatic-pressing treatments on the

transport critical current density. Journal of Applied Physics 70:1606–1613.

Yao YS, Guertin RP, Hinks DG, Jorgensen J, Capone DW (1988) Superconductivity of divalent Chevrel phases at very high pressures. Physical Review B 37:5032–5037.

Yeshurun Y, Malozemoff AP (1988) Giant flux creep and irreversibility in an Y-Ba-Cu-O crystal: An alternative to the superconducting-glass model. Physical Review Letters 60:2202–2205.

Youwen X, Suenaga M (1991) Irreversibility temperature in superconducting oxides: The flux-line-lattice melting, the glass-liquid transition, or the depinning temperatures. Physical Review B 43:5516–5525.

Yvon K, Paoli A (1977) Charge transfer and valence electron concentration in Chevrel phases. Solid State Communications 24:41–45.

Zheng DN, Hampshire DP (1997) The effect of Gd doping on the critical current of the Chevrel phase superconductor $PbMo_6S_8$. IEEE Transactions on Applied Superconductivity 7:1755–1759.

Zheng DN, Ramsbottom HD, Hampshire DP (1995) Reversible and irreversible magnetization of the Chevrel-phase superconductor $PbMo_6S_8$. Physical Review B 52:12931–12938.